https://doi.org/10.5194/bg-2020-454
Preprint. Discussion started: 8 January 2021

Biogeosciences Discussions

Reviews and syntheses: Ongoing and emerging opportunities to improve environmental science using observations from the Advanced Baseline Imager on the Geostationary Operational Environmental Satellites

Anam M. Khan[1], Paul C. Stoy[1,2,3,4], James T. Douglas[4], Martha Anderson[5], George Diak[6], Jason A. Otkin[6,7], Christopher Hain[8], Elizabeth M. Rehbein[9], Joel McCorkel[10]

[1]Nelson Institute for Environmental Studies, University of Wisconsin – Madison, Madison, WI, USA
[2]Department of Biological Systems Engineering, University of Wisconsin – Madison, Madison, WI, USA
[3]Department of Atmospheric and Oceanic Sciences, University of Wisconsin – Madison, Madison, WI, USA
[4]Department of Land Resources and Environmental Sciences, Montana State University, Bozeman, MT, USA
[5]USDA ARS, Hydrology and Remote Sensing Laboratory, Beltsville, MD, USA
[6]Space Sciences and Engineering Center, University of Wisconsin – Madison, Madison, WI, USA
[7]Cooperative Institute for Meteorological Satellite Studies, University of Wisconsin – Madison, Madison, WI, USA
[8]Short-term Prediction Research and Transition Center, NASA Marshall Space Flight Center, Earth Science Branch, Huntsville, AL, USA
[9]Department of Electrical and Computer Engineering, Montana State University, Bozeman, MT, USA
[10] NASA Goddard Space Flight Center, Greenbelt, MD, 20771, USA

Correspondence to: Anam M. Khan (amkhan7@wisc.edu)

Abstract. Environmental science is increasingly reliant on remotely-sensed observations of the Earth's surface and atmosphere. Observations from polar-orbiting satellites have long supported investigations on land cover change, ecosystem productivity, hydrology, climate, the impacts of disturbance, and more, and are critical for extrapolating ("upscaling") ground-based measurements to larger areas. However, the limited temporal frequency at which polar-orbiting satellites observe the Earth limits our understanding of rapidly evolving ecosystem processes, especially in areas with frequent cloud cover. Geostationary satellites have observed the Earth's surface and atmosphere at high temporal frequency for decades, and their imagers now have spectral resolutions in the visible and near-infrared regions that are comparable to commonly-used polar-orbiting sensors like the Moderate Resolution Imaging Spectroradiometer (MODIS), Visible Infrared Imaging Radiometer Suite (VIIRS), or Landsat. These advances extend applications of geostationary Earth observations from weather monitoring to multiple disciplines in ecology and environmental science. We review a number of existing applications that use data from geostationary platforms and present upcoming opportunities for observing key ecosystem properties using high-frequency observations from the Advanced Baseline Imagers (ABI) on the Geostationary Operational Environmental Satellites (GOES), which routinely observe the Western Hemisphere every 5 - 15 minutes. Many of the existing applications in environmental science from ABI are focused on estimating land surface temperature, solar radiation, evapotranspiration, and biomass burning emissions along with detecting rapid drought development and wildfire. Ongoing work in estimating vegetation properties and phenology from other geostationary platforms demonstrates the potential for expanding ABI observations to estimate vegetation greenness, moisture, and productivity at high temporal frequency across the Western

https://doi.org/10.5194/bg-2020-454
Preprint. Discussion started: 8 January 2021

Hemisphere. Finally, we present emerging opportunities to address the relatively coarse resolution of ABI observations through multi-sensor fusion to resolve landscape heterogeneity and to leverage observations from ABI to study the carbon cycle and ecosystem function at unprecedented temporal frequency.

1 Introduction

Modern environmental science would be unrecognizable without satellite remote sensing, which has revolutionized our field since its advent over a half-century ago (Kerr and Ostrovsky, 2003). The platforms by which we observe the Earth system are increasingly diverse and now include miniaturized satellites (CubeSats), sensors like ECOSTRESS traveling onboard the International Space Station (Hulley et al., 2017), and even lidar systems (Coyle et al., 2015; Qi et al., 2019), yet most environmental science applications employ polar-orbiting satellites, namely Landsat and the Moderate Resolution Imaging Spectroradiometer (MODIS). The Landsat and MODIS programs have radically improved the ability of ecologists to track vegetation change and its impacts on habitat, biogeochemical cycling, and other ecosystem services (De Araujo Barbosa et al., 2015). Like all remote sensing platforms, polar-orbiting satellites must make compromises with respect to spectral resolution, spatial scale, and temporal scale that limit their ability to 'measure all things, all the time'. Notably, the 1-to-2 day cadence of MODIS and VIIRS and 3-to-5 day cadence of the combined Landsat- and Sentinel-2-class sensors may be insufficient to track ecological phenomena that occur at shorter time scales, including the timing of rapid environmental change (White et al., 2009) and the diurnal behavior of land surface function (Chudnovsky et al., 2004; Grant et al., 2000).

As a part of the European Organization for the Exploitation of Meteorological Satellites (EUMETSAT), the Satellite Application Facility for Land Surface Analysis (LSA SAF) has leveraged high frequency observations from the Spinning Enhanced Visible and Infrared Imager (SEVIRI) onboard the Meteosat Second Generation (MSG) geostationary satellites to provide operational products relevant for studying vegetation, wildfires, the surface radiation budget, and the carbon and water cycle (Trigo et al., 2011) at sub-daily time scales. These opportunities are also available in the Western Hemisphere. Focusing on the Advanced Baseline Imager (ABI), a joint effort by the National Oceanic and Atmospheric Administration (NOAA) and the National Aeronautics and Space Association (NASA), onboard the Geostationary Operational Environmental Satellites (GOES), we argue that the GOES constellation – commonly used as weather satellites – represents an under-explored opportunity for environmental science in situations where spatial resolution can be compromised in favor of more frequent imagery, especially now that ABI's spectral sensitivity has approached that of Landsat and MODIS (Table 1; Fig. 1). Given the constellation of geostationary satellites around the world, extending environmental science applications to ABI and generating relevant data products is crucial for achieving near-global coverage of satellite environmental data available at the time scale of minutes. Developing algorithms that can be applied to data from multiple geostationary satellites will be an important component for achieving near-global coverage.

Here, we detail a number of applications by which geostationary satellites have enhanced or could enhance our understanding of ecological phenomena that occur at time scales as short as minutes. We outline the technical steps

https://doi.org/10.5194/bg-2020-454
Preprint. Discussion started: 8 January 2021

necessary to make imagery from ABI more useful for environmental science with an eye toward near real-time monitoring of environmental phenomena across the globe. We also note complementarity between GOES and other geostationary platforms including Japan's Himawari-8&9, South Korea's GEO-KOMPSAT-2A, and European Union Meteosat satellites – especially the forthcoming third-generation (MTG) – all of which have similar spectral resolution that make near-global observation possible (Table 1). We first review the recent efforts regarding geolocation and atmospheric correction to produce surface reflectance from ABI and other geostationary imagers. We then describe new data products that can be created using state-of-the-art geostationary satellite data with a brief description of existing data products that are providing key insight into Earth surface processes. Finally, we outline existing and emerging applications of observations from geostationary satellites that are ushering in the era of 'hyper-temporal' remote sensing (Miura et al., 2019) for environmental science.

2 Background

2.1 Geostationary satellites: Past, present, and future

Geostationary remote sensing began with the launch of six Applications Technology Satellites (ATS) starting in 1966 (Suomi and Parent, 1968). The subsequent successful launches of the Synchronous Meteorological Satellites (SMS) were the precursor to the GOES mission, which began in 1974 and continues to the present (Menzel, 2020). By 1979, the global constellation of geostationary satellites included the European Space Agency's Meteosat, the Japanese Geostationary Meteorological Satellite (GMS), and two GOES (Menzel, 2020). Seventeen GOES have been successfully sent to space as of 2018, two of which – GOES-16 positioned at 75.2 W (currently GOES-East) and GOES-17 positioned at 137.2 W (currently GOES-West) – arise from the GOES-R Series that include additional visible and near-IR channels that are commensurate with channels observed by Landsat and MODIS (Table 1, Figure 1). The GOES-R Series has an expected operational lifetime to 2036 which promises multiple years of continuous data availability. This will be followed by the Geostationary and Extended Orbits program, which is planned for operation in 2030-2050 and is anticipated to include "GOES-R-class" imagers (Sullivan et al., 2020).

2.2 Advanced Baseline Imager (ABI)

The ABI is the primary instrument onboard GOES-16/17 and is designed for monitoring land and ocean surfaces, the atmosphere, and cloud formation (Schmit et al., 2017, 2018). The ABI has 16 spectral bands that measure solar reflected radiance in the visible and near-infrared wavelengths and emitted radiance at infrared wavelengths (Schmit and Gunshor, 2020). With multiple infrared bands positioned in atmospheric absorption regions and in atmospheric windows, the ABI can collect information from the Earth's surface and multiple levels in the atmosphere (Schmit and Gunshor, 2020). Multiple scan modes are used to provide near-hemispheric geographic coverage with spatial resolutions between 0.5 and 2 km. The full disk scene consists of near hemispheric coverage centered at the equator and the longitude of the sensing satellite (DOC,

https://doi.org/10.5194/bg-2020-454
Preprint. Discussion started: 8 January 2021

NOAA, NESDIS, NASA, 2019). The ABI also scans a scene of the contiguous United States (CONUS) and two mesoscale scenes (1000 km by 1000 km). Operating in the flex mode, ABI collected a full disk image every 15 minutes until April 2019 but now collects a full disk image every 10 minutes (with the exception of GOES-17 during parts of the year). ABI also collects a CONUS scene every 5 minutes, and two mesoscale scenes every minute in the flex mode (Schmit and Gunshor, 2020).

In late April 2018, an issue with the GOES 17 ABI cooling system was detected due to malfunctioning of the loop heat pipe which transfers heat from the ABI detectors and helps maintain adequate temperatures for proper functioning (Yu et al., 2019). This results in the loss of infrared data during some nighttime hours around 13:30 UTC in parts of the year due to the sun heating the 7 ABI detectors faster than they can be cooled resulting in infrared emissions from the overheated detectors (NOAA; NOAA and NASA). This nighttime data loss can also fluctuate seasonally depending on how much solar radiation the instrument absorbs (NOAA). A data quality flag in the metadata of the Level 1b radiances and Level 2 Cloud and Moisture Imagery can identify the faulty nighttime data (NOAA and NASA). This malfunction will result in the loss of some nighttime data for data products that utilize the infrared bands and are relevant for observing the full diurnal cycle.

3 Working with ABI data

The ABI collects top-of-atmosphere (TOA) data from a certain location on the Earth at a constant view zenith angle (VZA) and varying solar zenith angles (SZA) throughout the day. While the increased sampling of SZA creates opportunities in surface Bidirectional Reflectance Factor (BRF) modeling (Ma et al., 2020), the large VZA at off-nadir locations can present challenges for studying the land surface including coarsened resolution, potentially degraded locational accuracy, and more complex atmospheric compensation due to longer slant paths. Below, we review the existing efforts to address these challenges and make ABI imagery more suitable for studying the land surface.

3.1 Geolocation

The geolocation accuracy of ABI on GOES-16 and GOES-17 has been tracked and improved throughout its provisional and operational stages using the Image Navigation and Registration Performance Assessment Tool Set (IPATS) (Tan et al., 2018, 2019, 2020). IPATS can quantify the navigation error, which is the difference between the location of a pixel in ABI imagery and its true location (Tan et al., 2020). Some of the largest navigation errors, calculated from correlations between subsets of ABI and Landsat 8 imagery concentrated along the coast of North and South America, were 10 - 13 μrad less than the mission requirement of 28 μrad (1 km at nadir) in October 2019 (Tan et al., 2020). In addition to IPATS, the Geostationary-NASA Earth Exchange (GeoNEX) processing chain adjusts the geolocation of ABI imagery using a reference map from the Shuttle Radar Topographic Mission (SRTM) Digital Elevation Model (DEM) and more than 30,000 landmarks along coastlines (Wang et al., 2020). The shift in the geolocation of the red band (500 m at nadir) between IPATS and the GeoNEX algorithm was under 0.5 pixels for a majority of the time throughout the full disk scene but can be as large as 1 - 2 pixels for short periods of time (Wang et al., 2020).

https://doi.org/10.5194/bg-2020-454
Preprint. Discussion started: 8 January 2021

3.1 Parallax

Geostationary satellites observe most of the hemisphere at an angle relative to the zenith, which introduces a challenge due to parallax: the effect of observing an object from a large VZA. Parallax can result in uncertainties in land surface observations in mountainous terrain and can introduce errors in the mapped location of clouds (Bieliński, 2020; Good, 2015). These errors vary by VZA and the height of the feature and are largest for high VZA and high feature altitude relative to the surface (Bieliński, 2020; Zakšek et al., 2013). For example, the parallax shift at 49 degrees latitude from GOES-16 ABI can be as large as 51 km for an object that is 15 km high (Whittaker 2014). Since the mapped location of the clouds detected depends, in part, on the VZA, parallax shifts can also complicate comparing the location of clouds between sensors with different VZA (Zakšek et al., 2013). However, it is possible to correct for parallax shifts with knowledge of VZA and feature (cloud or surface) altitude (Kim et al., 2017; Yeom et al., 2020).

3.3 Atmospheric correction

3.3.1 Surface reflectance

Correcting for atmospheric attenuation of radiation to derive surface reflectance from TOA reflectance is a crucial prerequisite to studying surface processes for any satellite platform. Current efforts to estimate surface reflectance from ABI, Advanced Himawari Imager (AHI), and the Geostationary Ocean Color Imager (GOCI) onboard the Communication, Ocean, and Meteorological Satellite (COMS) include generating lookup tables from the Second Simulation of the Satellite Signal in the Solar Spectrum (6S) radiative transfer model (He et al., 2019; Tian et al., 2010; Vermote et al., 1997; Yeom et al., 2018, 2020; Yeom and Kim, 2015). Optimal estimation methods that estimate surface BRF from SEVIRI have been extended to estimate surface broadband albedo and surface reflectance from ABI and the AHI on Himawari-8 (Govaerts et al., 2010; He et al., 2019, 2012; Wagner et al., 2010). These algorithms estimate surface reflectance and broadband surface albedo by minimizing the difference between TOA BRF estimated through radiative transfer modeling and measured by the satellite (He et al., 2019, 2012). Unlike the surface reflectance algorithm currently used for SEVIRI, the algorithm for ABI and AHI takes the diurnal variation of aerosol optical depth into account (He et al., 2019). Originally developed for atmospheric correction of MODIS imagery, the Multi-Angle Implementation of Atmospheric Correction (MAIAC) has also been adapted to provide provisional daytime surface reflectance every 10 minutes for bands 1 - 6 of AHI with plans to extend the algorithm to ABI (Li et al., 2019b). The surface reflectance from AHI showed less variation compared to surface reflectance from MODIS and the differences in surface reflectance between AHI and MODIS were smaller for the red, near-infrared (NIR), and shortwave infrared (SWIR) bands compared to the blue and green bands (Li et al., 2019b). ABI channels 1, 3, 5, and 6 are accurate to within 2% but channel 2 has a bias error of up to 5% (McCorkel et al., 2020). With geolocation, parallax, atmospheric correction, and sensor accuracy taken into account, imagery from ABI can provide diurnal estimates of various land surface variables.

https://doi.org/10.5194/bg-2020-454
Preprint. Discussion started: 8 January 2021

3.3.2 Surface temperature

Since the emission from the land surface diverges from a blackbody, the knowledge of land surface emissivity is a crucial component of retrieval of surface temperature from at-sensor radiance (Li et al., 2013; Sun and Pinker, 2003). Global emissivity data may be gathered by consulting compiled tables of emissivities for various land covers along with land cover classifications of the landscape (Li et al., 2013). Land surface emissivity can also be estimated through its relationship with the normalized difference vegetation index. This method only applies to vegetation and soil and requires knowledge about the fractional cover of vegetation in a pixel (Li et al., 2013). Furthermore, land surface emissivities can be estimated by using surface temperature-emissivity separation techniques applied to multi-spectral thermal satellite observations (Li et al., 2013). Various methods have been developed to retrieve surface temperature depending on if surface emissivity is known or unknown a priori (Li et al., 2013).

A single-channel approach requires the use of one thermal channel within an atmospheric window at around 10 μm and radiative transfer modeling to simulate atmospheric transmittance and emission of longwave radiation (Li et al., 2013; Pinker et al., 2019). With known land surface emissivity and atmospheric profiles and simulated atmospheric transmittance/emission, surface temperature can be retrieved through the inversion of a radiative transfer equation that explains the different components of at-sensor radiance (Li et al., 2013). Since accurate atmospheric profiles over the study area can be difficult to obtain, a split-window technique can be used to correct atmospheric absorption to estimate surface temperature from at-sensor radiance in two thermal bands with differential water vapor absorption (Li et al., 2013; Ulivieri and Cannizzaro, 1985). Split-window techniques are based on the relationship between surface temperature and the difference in temperature between two adjacent thermal bands with high emissivity and low atmospheric absorption typically centered at 11 and 12 μm (Li et al., 2013; Sun and Pinker, 2003). Section 4.4 further expands on the use of single and multiple channel surface temperature retrieval techniques to estimate land surface temperature from geostationary satellites.

4 Data products

Geostationary satellites can measure a number of common indices used for ecological applications and make measurements that support derived products including land surface temperature and incident solar radiation. We describe these measurements with an eye toward explaining the benefits and disadvantages of using geostationary platforms for ecological applications.

4.1 Incident solar radiation and Photosynthetically Active Radiation (PAR)

Geostationary satellites are equipped to estimate incident solar radiation at the Earth's surface (Diak, 2017; Pinker et al., 2002), critical for the surface energy balance, photosynthesis, and solar power applications. Earlier efforts to do so include a simple physical model by Gautier et al. (1980) which estimated incident solar radiation during clear and cloudy conditions using the reflectance from the visible band of the Visible Infrared Spin Scan Radiometer (VISSR) on GOES-2. The model

https://doi.org/10.5194/bg-2020-454
Preprint. Discussion started: 8 January 2021

included Rayleigh scattering and water vapor absorption of downwelling and reflected shortwave radiation. Cloud albedo and absorption were estimated from a linear relationship with the satellite-measured cloud reflectance and estimates of incident solar radiation were subsequently improved by including ozone absorption of shortwave radiation in the atmosphere (Diak, 2017; Diak and Gautier, 1983). Continued improvements in both the physical model and the spatiotemporal resolution of the GOES imagery have resulted in higher accuracy of hourly and daily insolation estimates when compared to pyranometer measurements (Diak, 2017; Otkin et al., 2005). More recent models of the transmittance of direct and diffuse shortwave radiation through aerosol extinction by different aerosol components, gaseous absorption, and Rayleigh scattering have provided estimates of the surface shortwave radiation flux and its diffuse fraction from SEVIRI observations at 15-min resolution (Carrer et al., 2019) and could also be applied to ABI observations. Applying algorithms for estimating incident solar radiation to data from multiple geostationary satellites can lead to near-global coverage and be beneficial for near-global estimates of evapotranspiration and gross primary productivity.

Incident solar radiation in the wavelengths of Photosynthetically Active Radiation (PAR, 400 - 700 nm) can also be estimated using the visible bands of geostationary satellites (Janjai and Wattan, 2011). Given a set of illuminating/viewing angles, cloud type, aerosol type, cloud extinction coefficient, and atmospheric visibility, lookup tables generated from simulations of Moderate Resolution Atmospheric Transmission (MODTRAN) have been used to estimate downwelling PAR from at-sensor radiance (Zhang et al., 2014; Zheng et al., 2008). These methods have been extended to multiple geostationary satellites and MODIS surface reflectance data to generate global incident PAR estimates (Zhang et al., 2014). Although these methods account for elevation, validation efforts have shown that satellite-derived PAR in high-altitude areas can be biased when compared to ground measurements, possibly due to inaccurate specification of atmospheric profiles governing water vapor corrections (Zhang et al., 2014). Furthermore, PAR estimated from satellites has been reported to underestimate PAR measured on the ground when the model assumed urban aerosol absorption over areas where maritime aerosols were more dominant (Janjai and Wattan, 2011). Despite these limitations, frequent estimates of PAR and incident solar radiation from geostationary satellites may be uniquely suited to drive the land surface models that are operating at increasingly fine spatial and temporal resolutions, providing a natural link for using geostationary satellite observations to improve our understanding of the carbon, water, and energy cycles (Williams et al., 2009).

Terrestrial photosynthesis is particularly responsive to diffuse PAR, which penetrates plant canopies more efficiently than direct PAR (Emmel et al., 2020; Gu et al., 2003). The diffuse fraction of incoming PAR is well-described as a linear function of transmissivity, or a clearness index, through the atmosphere within certain inflection points (Erbs et al., 1982; Oliphant and Stoy, 2018; Weiss and Norman, 1985). Estimates of cloud height, optical depth, and particle size along with aerosols from GOES can be used to further partition incoming PAR into direct and diffuse beam fractions as currently provided by EUMETSAT at 15-minute intervals (Carrer et al., 2019). Such observations could ultimately prove useful for analyses of the diurnal pattern of carbon cycling (see section 6.1), given that the variability in terrestrial carbon cycling is often most sensitive to the variability of PAR at time scales from minutes to days (Stoy et al., 2005).

https://doi.org/10.5194/bg-2020-454
Preprint. Discussion started: 8 January 2021

4.2 Vegetation greenness

The Normalized Difference Vegetation Index (NDVI) – the normalized difference between the reflectance in red and near-infrared wavelengths – is strongly correlated to chlorophyll content, green biomass, leaf area index (LAI), and the fraction of incoming PAR absorbed by leaves (fAPAR) (Gamon et al., 1995; Jordan, 1969; Rouse et al., 1974; Running et al., 1986; Tucker, 1979; Tucker et al., 1985) and therefore is a critical variable for monitoring the land surface. ABI has the ability to also measure the Enhanced Vegetation Index (EVI) which is preferred for some carbon cycle applications in areas (and periods) of dense vegetation cover where, unlike NDVI, EVI does not saturate (Huete et al., 2002; Zhou et al., 2014). The near-infrared reflectance of vegetation (NIRv) is strongly correlated to the amount of incoming PAR absorbed by plants and therefore photosynthesis at half-hourly to annual timescales and has shown stronger relationships with photosynthesis compared to NDVI (Badgley et al., 2017, 2019; Baldocchi et al., 2020; Wu et al., 2020).

High temporal estimates of LAI from ABI will have widespread utility by providing an important variable needed for modeling seasonal vegetation dynamics and energy, water and carbon fluxes (Anderson et al., 2011; Guan et al., 2014; Robinson et al., 2018). An ABI LAI product can provide harmony in temporal scales and data sources needed to estimate fractional vegetation cover needed for a two-source energy balance model used for estimating evapotranspiration from GOES thermal data (further discussion in section 5.1) (Anderson et al., 2011). Similarly, the ABI LAI product can provide a data source for plant respiration modeling in future modeling of carbon fluxes from ABI (further discussion in section 6.1) (Robinson et al., 2018). LAI along with other biophysical parameters such as fractional vegetation cover and fAPAR are produced at daily and 10-day time scales through the LSA SAF program (Trigo et al., 2011). The methodology of Roujean and Lacaze (2002) is used to obtain LAI from an exponential relationship with fractional vegetation cover.

The increased temporal frequency of measurements available from geostationary satellites compared to polar-orbiting satellites provide more opportunities for measuring NDVI, EVI, LAI, and NIRv in areas with frequent cloud and snow cover (Miura et al., 2019). However, the geostationary position captures reflected radiation at varying SZA throughout the day and these novel sun-sensor geometries, not previously captured by polar orbiting satellites, can cause diurnal variation in vegetation indices calculated from TOA reflectance (Tran et al., 2020). In Australia, compared to NDVI, EVI shows less SZA induced diurnal variation and is less impacted by the midday hot spot effect during times of the year (spring and autumn equinox) when the SZA and AHI VZA are aligned (Tran et al., 2020). NDVI measurements can be normalized to a reference sun-target-sensor geometry by estimating bidirectional reflectance distribution functions (BRDF) to address the impacts of varying sun-sensor geometry (Fensholt et al., 2006; Seong et al., 2020; Tian et al., 2010; Yeom et al., 2018; Yeom and Kim, 2015). Given the SZA sensitivity of NDVI measurements, Wheeler and Dietze (2019) demonstrated a Bayesian model to estimate a daily midday NDVI value from diurnal NDVI calculations using ABI observations, which showed promising results for measuring NDVI at rapid time scales.

https://doi.org/10.5194/bg-2020-454
Preprint. Discussion started: 8 January 2021

4.3 Vegetation moisture

Liquid water absorption influences reflectance by plants in the atmospheric windows of shortwave infrared (SWIR) wavelengths (1.3 - 2.5 μm). Reflectance by plants in the SWIR has a negative relationship with leaf water content (Chen et al., 2005; Gao, 1996; Tucker, 1980), and multiple vegetation indices have been developed from bands in the SWIR wavelengths to capture these phenomena, especially in the 1.55 - 1.75 μm bands (Fensholt and Sandholt, 2003; Tucker, 1980). Some notable vegetation indices that use SWIR wavelengths are the Normalized Difference Infrared Index (NDII) and the Normalized Difference Water Index (NDWI) which have been formulated from the difference in reflectance (ρ) in the NIR (0.76 - 0.9) and SWIR (1.55 - 2.5 μm) bands as: (ρNIR - ρSWIR) / (ρNIR + ρSWIR) (Chen et al., 2005; Fensholt and Sandholt, 2003; Gao, 1996; Hardisky et al., 1983; Tucker, 1980). NDII has been used to improve global estimates of canopy water content and provided more realistic estimates of canopy water content in semiarid shrublands when compared to regression models without NDII (García-Haro et al., 2020). NDWI has been useful in estimating the water content of corn (maize) fields because it saturates at higher values than NDVI in response to changing vegetation water content during the growing season (Chen et al., 2005; Jackson et al., 2004). The shortwave infrared water stress indices derived from MODIS have stronger correlations with growing season soil moisture than NDVI in the semiarid grasses of northern Senegal, Africa (Fensholt and Sandholt, 2003). Many of these indices and their changes over time can now in principle be measured by geostationary satellites (Table 1).

ABI, along with the Advanced Meteorological Imager (AMI) on GEO-KOMPSAT-2A, AHI, and SEVIRI, all offer bands in the SWIR regions, with ABI band 5 placed in the refined interval of 1.55 - 1.75 μm identified by Tucker (1980) (Table 1). Atmospherically corrected surface reflectances from ABI, SEVIRI, AHI, and AMI can provide near-real-time and near-global coverage for vegetation water content. This remains a relatively unexplored opportunity given the potential benefits of near-real-time monitoring of vegetation status (Verger et al., 2014).

4.4 Land surface temperature

The ABI features three longwave infrared bands with spatial resolutions of about 2 km for measuring land surface temperature (LST) – the skin temperature of the uppermost layer of the land surface – including correction for atmospheric moisture (Yu et al., 2012). Determination of a physical surface temperature rather than an effective surface temperature is critical for many applications and, as previously discussed, requires knowledge of the surface emissivity (Yu et al., 2009, 2012). Data sources for land surface emissivity in LST retrievals from geostationary satellites can include spectral libraries given a specific type of environmental surface (Peres and DaCamara, 2005), the MODIS operational land surface emissivity product (MOD11) or the Combined ASTER and MODIS Emissivity over Land (CAMEL) product (Pinker et al., 2019).

The hourly ABI LST product uses the difference between the brightness temperatures of ABI bands 14 (11.2 μm) and 15 (12.3 μm) in a split-window algorithm with an added term to correct for path length at high view zenith angles (Yu et al., 2009, 2012). These bands were chosen because they are placed in regions of maximum surface emission with low

https://doi.org/10.5194/bg-2020-454
Preprint. Discussion started: 8 January 2021

atmospheric absorption (Yu et al., 2009). However, water vapor absorption in a more moist atmosphere (e.g. a water vapor content greater than 2 g cm^{-2}) at large view zenith angles (> 45°) remains an issue for the ABI LST algorithm (Yu et al., 2009).

For the generation of a consistent long-term record of LST, a single channel approach has also been proposed for LST retrieval from GOES 12 channel 4 (10.7 μm) in order to develop an algorithm that can be applied to data from multiple GOES satellites including for time periods from mid-2004 - 2017 when only one thermal channel was available (Pinker et al., 2019). Diurnal LST time series available from geostationary platforms have a wide range of applications in environmental monitoring, from mapping surface-atmosphere fluxes of heat, water, and carbon dioxide to tracking drought and fire dynamics. These and other applications are discussed further in the following sections.

5 Existing applications of geostationary satellites for environmental science

5.1 Evapotranspiration, latent heat flux, and sensible heat flux

Diurnal observations from GOES provide multiple estimates of directional surface radiometric temperature and downwelling solar radiation per day to estimate water and energy fluxes from the soil and canopy (Diak and Stewart, 1989). One approach for estimating evapotranspiration (ET) that is well-suited for geostationary implementation is the Atmosphere-Land Exchange Inverse (ALEXI) model (Anderson et al., 1997, 2007a; Mecikalski et al., 1999), which estimates the bulk surface energy balance (net radiation, sensible heat flux, latent heat flux, and soil heat flux) as well as the nominal partitioning of these fluxes between the soil and canopy. ALEXI is a time-integrated model based on the two-source (vegetation and soil) energy balance (TSEB) approach of Norman et al. (1995). ALEXI models the growth and sensible heating of the atmospheric boundary layer based on the morning rise in surface radiometric temperature that can be measured from geostationary platforms, estimating time-integrated latent heat flux (or ET in units of mass flux) as a residual to the overall energy balance (Anderson et al., 1997). The model performs best when the insolation inputs are also derived from geostationary satellite data (Sec. 4.1), giving optimal spatial and temporal correspondence between net radiation forcings and surface temperature response signals. In comparison with other sources of insolation data, geostationary-based insolation could improve significantly ET retrievals particularly in areas of frequent cloud cover where reanalysis estimates may not accurately capture the timing and spatial extents of clouds (Anderson et al., 2019; S. Ha et al., 2020).

ALEXI-based ET estimates are produced routinely at 4 km resolution for the United States (Anderson et al., 2020). Also, daily 2-km resolution ALEXI-based ET estimates have been generated from ABI observations as a part of the GOES ET and Drought (GET-D) product system (Fang et al., 2019). A surface energy balance approach has also been used to estimate 30-minute ET from albedo and downwelling radiation from MSG SEVIRI over the areas covered by MSG and 3-hourly ET in the Haihe River Basin in China from hourly LST observations from MTSAT, a Japanese geostationary satellite (Ghilain et al., 2011; Zhao et al., 2019). By measuring LST, geostationary satellites can estimate sensible heat flux and therefore also the Bowen ratio, which can give insight into atmospheric boundary layer heat and moisture transport as well as

https://doi.org/10.5194/bg-2020-454
Preprint. Discussion started: 8 January 2021

plant water stress (Diak and Whipple, 1995). Applications of ALEXI-based ET and energy fluxes for drought monitoring and modeling carbon fluxes are discussed below.

5.2 Drought monitoring

LST can change rapidly as a function of time, and LST retrieved using geostationary satellite-based thermal infrared (TIR) observations may provide early signals of developing drought stress (Otkin et al., 2013). The Evaporative Stress Index (ESI; Anderson et al., 2013) represents standardized anomalies in a reference ET fraction that is computed using satellite-derived actual ET estimates from the ALEXI model. ESI has proven to be an effective indicator of moisture stress in vegetation (Anderson et al., 2007b, 2013, 2016; Otkin et al., 2015, 2018a) and the onset of flash drought conditions characterized by a period of rapid drought intensification (Otkin et al., 2014, 2016, 2018b). Flash drought conditions typically include warm air temperature and low cloud cover anomalies, with dew point suppressions and high winds that can hasten ET and remove water from ecosystems.

Drought indicators based on remotely sensed TIR observations can improve the effectiveness of drought early warning systems due to their high spatial resolution and the tendency for large decreases in ET to precede visible reductions in vegetation biomass during early stages of drought development (Anderson et al., 2013; Otkin et al., 2015). The ESI has also been used as a moisture stress indicator for estimating drought impacts on crop yields (Anderson et al., 2016a, b). ESI is routinely generated at 4 km resolution over the CONUS, and 5 km globally.

5.3 Wildfire detection and biomass burning emissions

The Automated Biomass Burning Algorithm (ABBA) was developed from the 4 μm and 11 μm bands of the GOES visible infrared spin scan radiometer atmospheric sounder (VAS) to identify fire pixels (Prins and Menzel, 1994) based on the differential increases in emitted radiation with increases in temperature between the two bands. The ABI fire algorithm has adapted ABBA to detect fires from differences in the brightness temperatures of the 3.9 μm and 11.2 μm bands and provides the location, sub-pixel size, temperature, and radiative power of fires (Schmidt et al., 2012; Schmit et al., 2015). Fire Radiative Power (FRP) is the rate at which radiation is emitted from a fire and, for a 600 - 1400 K temperature range, FRP is proportional to the difference between radiance in the middle infrared (MIR) at 3.9 μm and the regional background radiance in MIR (Schmidt et al., 2012; Wooster, 2003; Xu et al., 2010). Fire Radiative Energy (FRE) is the time-integrated FRP during the course of a fire. Emissions of trace gasses and aerosols from biomass burning can be estimated using FRE, a biomass combustion rate, and an emission factor specific to land cover and emitted species (Zhang et al., 2012). The diurnal FRP cycles of various ecosystems have been estimated from GOES and from fusion of FRP estimates from GOES and MODIS to provide biomass burning emissions at hourly, daily, and monthly scales (Li et al., 2019a; Zhang et al., 2012).

https://doi.org/10.5194/bg-2020-454
Preprint. Discussion started: 8 January 2021

5.4 Plant phenology

Plant canopies have unique and observable events that occur annually as a part of their phenology. There is a long history of observing these annual events, and richly-documented historical (non-satellite) datasets exist in some locations for time periods spanning multiple centuries (Aono and Kazui, 2008). The phenology of photosynthesis and plant growth is sensitive to temperature, precipitation, and photoperiod (Bauerle et al., 2012; Fu et al., 2017; Piao et al., 2019; Stoy et al., 2014a), and shifts in the phenology of carbon uptake and plant growing season in response to changing climate have important implications for ecosystems (Bradley et al., 1999; Xu et al., 2020). These shifts often occur on time scales that cause uncertainty from polar-orbiting satellites, especially when cloudy conditions are present during spring in the temperate zone (Richardson et al., 2013) and dry-to-wet (and wet-to-dry) seasonal transitions in tropical forests (Ganguly et al., 2010).

Research on land surface phenology to date has used a combination of satellite remote sensing and near-surface remote sensing via webcams to detect seasonal transitions in vegetation greenness and photosynthesis such as the start, peak, and end of the growing season (Dannenberg et al., 2020; Gamon et al., 2016; Seyednasrollah et al., 2019; Wong et al., 2019; Zhang et al., 2003). These observations have varying spatial and temporal resolutions depending on the method and instrumentation used (Brown et al., 2016; Filippa et al., 2018; Liu et al., 2017).

Geostationary satellites such as GOES have unique capabilities that could further enhance plant phenology research. Compared to polar-orbiting satellites, the large number of diurnal observations from geostationary satellites capture greater variation in sun-angle geometries. This increased variability allows for better BRDF adjustments and improved investigations about the impact of the SZA on the vegetation indices used for extracting phenological transitions (Ma et al., 2020). Time series of LAI, NDVI, and the two-band Enhanced Vegetation Index (EVI2) from SEVIRI, AHI, and GOCI show increased observations during cloudy conditions and improved estimates of phenological cycles and transitions (Guan et al., 2014; Miura et al., 2019; Yan et al., 2016; Yeom et al., 2018; Yeom and Kim, 2015). For example, NDVI from BRDF-adjusted reflectance from GOCI has demonstrated an improved ability to monitor the growth of rice paddies in North Korea and South Korea compared to MODIS NDVI from BRDF adjusted reflectance, especially during the monsoon season with frequent cloud cover that limits the ability of polar-orbiting sensors to observe the surface (Yeom et al., 2015, 2018). In the Congo Basin, the multiple annual phenological cycles of greenness in evergreen broadleaf forests were better captured by the increased observations from SEVIRI compared to MODIS (Yan et al., 2016). Leveraging diurnal observations from GOES to estimate phenological transitions (Wheeler and Dietze 2020) across the Western Hemisphere coupled with the ability to extract these transitions from AHI, SEVIRI, and GOCI can result in a near-global improvement in estimating seasonal vegetation growth and decline. The capacity of GOES to track events in plant phenology is shown in Figs. 3 and 4 for the Kincade Fire example with notable increases in vegetation greenness and moisture during March and April at the end of the typical rainy season in California's Mediterranean ecosystems.

https://doi.org/10.5194/bg-2020-454
Preprint. Discussion started: 8 January 2021

5.5 Ocean color

Geostationary satellites have been used for nearly a decade for monitoring the dynamics of ocean color. The ocean color signal can identify suspended particulate matter and phytoplankton (Neukermans et al., 2009; Ruddick et al., 2014) including harmful algal blooms (Choi et al., 2014; Noh et al., 2018) and may be a sentinel for the impacts of climate change on marine ecosystems (Dutkiewicz et al., 2019). Most research to date has involved the Geostationary Ocean Color Imager (GOCI), which has transmitted eight images per day since 2010 in six visible (412, 443, 490, 555, 660, and 680 nm) and two infrared channels (745 and 865 nm) with 20 nm bandwidth at 500 m spatial resolution centered around the Korean Peninsula at 128.2 °E (Ahn et al., 2012; Choi et al., 2012; Ryu et al., 2012; Ryu and Ishizaka, 2012) (Table 1). GOCI has been used to estimate ocean biogeochemical dynamics (Wang et al., 2013) including photosynthesis via chlorophyll-a absorption (Concha et al., 2018; Park et al., 2012) at diurnal time scales. Other geostationary sensors including SEVIRI on the 2nd generation of METEOSAT (Schmetz et al., 2002) and (forthcoming) flexible combined imager (FCI) on the 3rd generation of METEOSAT (Ouaknine et al., 2013) are not designed explicitly for ocean color monitoring but have proven useful for monitoring marine suspended particulates and PAR attenuation in water (Neukermans et al., 2009; Ruddick et al., 2014) as has GOES (Jolliff et al., 2019). All of these sensors provide an important complement to ocean color monitoring from polar-orbiting satellites like MODIS-AQUA, MERIS, and the Ocean Land Color Instrument (OLCI) on Sentinel-3 (Nieke et al., 2012; Peschoud et al., 2017). The persistent and consistent atmospheric characterization afforded by the geostationary sensors is critical for interpreting the relatively weak marine color signature (Ruddick et al., 2014).

6 Emerging Applications

6.1 Carbon cycle science

Estimates of surface-atmosphere carbon flux from polar-orbiting instruments like MODIS are usually produced on 8-day to annual time steps (Zhao et al., 2005). The impact of rapidly evolving meteorological conditions on terrestrial carbon uptake has gained recent attention, suggesting that more frequent observations will improve our understanding of the carbon cycle. Precipitation events and the resulting short-term changes in meteorological conditions on the order of days result in local anomalies in canopy photosynthesis and respiration that influence seasonal ecosystem exchange (Randazzo et al., 2020). Fluctuations in carbon uptake can result from upwind climate extremes through heat and moisture advection, revealing more complexity in how climate extremes impact ecosystem carbon fluxes (Schumacher et al., 2020). Smoke from large wildfires can result in a short-term decrease in incoming PAR but an increase in the diffuse fraction of incoming PAR which, under the right circumstances, can increase seasonal carbon uptake through changes in Light-Use Efficiency (LUE, Hemes et al., 2020). The resulting daily anomalies in gross primary productivity (GPP) from sudden changes in limiting resources have been shown to disproportionately affect longer-term ecosystem carbon uptake (Kannenberg et al., 2020). Multi-day positive anomalies in GPP are critical for explaining its interannual variation at ecosystem and global scales (Fu et al., 2019;

https://doi.org/10.5194/bg-2020-454
Preprint. Discussion started: 8 January 2021

Zscheischler et al., 2016). All of these recent findings point to the importance of more frequent observations of ecosystem carbon cycling to improve our understanding of global carbon cycling.

Now that geostationary satellite imagers measure similar spectral bands to MODIS (Fig. 1, Table 1), they can be used to monitor the carbon cycle in similar ways but at higher temporal frequency. The MODIS GPP algorithm for example uses LUE logic based on a linear relationship between absorbed PAR (APAR) and net primary production (NPP) (Monteith, 1972; Running et al., 2004; Zhao et al., 2005). It uses NDVI to estimate APAR then estimates GPP using a light-to-carbon conversion efficiency parameter (ε_{max}) adjusted for conditions in which temperature (T_{scale}) or water stress (W_{scale}) limit GPP using a Jarvis (1976)-type formulation (Zhao et al., 2005). T_{scale} and W_{scale} vary between 0 and 1 and all three parameters vary by ecosystem type. The Vegetation Photosynthesis and Respiration Model (VPRM) (Mahadevan et al., 2008) uses a similar approach and estimates gross ecosystem exchange (GEE, similar to GPP) using the Enhanced Vegetation Index (EVI) instead of NDVI. The Land Surface Water Index (LSWI), the normalized difference between satellite-derived reflectance in near-infrared and shortwave infrared, is used to adjust LUE in response to water stress and leaf phenology (Mahadevan et al., 2008). Multiple additional approaches for estimating GPP from space exist and often use the LUE approach with differences arising from the spatio-temporal resolution of the inputs, the meteorological data used, incorporating the impacts of CO_2 fertilization, environmental scalars used for adjusting LUE, and the treatment of LUE as a constant or specific to biome, plant functional type, or photosynthetic pathway (McCallum et al., 2009; Robinson et al., 2018; Sims et al., 2006; Xiao et al., 2019).

Implementing a model to estimate GPP from ABI presents opportunities to improve LUE-based models by incorporating the impacts of diffuse radiation on LUE and investigating emerging variables, as opposed to the commonly used air temperature and vapor pressure deficit, to represent environmental stressors on ε_{max} such as LST and the evaporative fraction (Anderson et al., 2000; Yuan et al., 2007). Ecosystem GPP increases with increases in diffuse radiation if light does not limit photosynthesis because diffuse radiation penetrates plant canopies more readily resulting in a more even distribution of light among shaded and sunlit leaves. (Hemes et al., 2020; Mercado et al., 2009). Incorporating the diffuse component of incoming PAR has been noted as a priority for the new generation of GPP models (McCallum et al., 2009). Partitioning estimates of PAR from ABI into diffuse and direct components along with the ABI LST product and ALEXI based estimates of sensible and latent heat flux can provide harmony between inputs for environmental stressors on ε_{max}, PAR, and vegetation indices by not having to rely on estimates from sources other than ABI. Furthermore, estimates of LAI from GOES can contribute to respiration modeling data needs for estimating NPP (Robinson et al., 2018). Observations from geostationary satellites could also, in principle, be used to assimilate instantaneous carbon flux observations from eddy covariance towers into ecosystem models (LeBauer et al., 2011).

6.2 Disturbance and recovery

Remotely sensed data have made it possible to map regional burn severity from wildfires, while time series of measures of greenness and primary productivity enable monitoring of vegetation disturbance and recovery (Bolton et al., 2017; Goetz et

https://doi.org/10.5194/bg-2020-454
Preprint. Discussion started: 8 January 2021

al., 2006; Meng et al., 2018). Mapping damage from hurricanes and the resulting impact to the carbon cycle has also been possible using remotely sensed data through the use of various vegetation indices related to greenness and moisture (Chambers et al., 2007; Wang et al., 2010). The difference in NDVI from pre- and post-fire imagery from GOES-16 shows the potential to detect variation in burn severity and recovery from wildfires as demonstrated for the notable Kincade Fire in 2019 in California (Fig. 2). High-frequency estimates of NDVI (Fig. 3) and NDII (Fig. 4) from GOES-16 can track vegetation disturbance and recovery from wildfire in a similar manner to MODIS and the dense time series of GOES data is notably less variable than MODIS for pixels within and outside – and before and after – the Kincade Fire (Fig. 3). Variations in SZA and VZA can lead to differences in NDVI values between GOES, MODIS, and other sensors (Fensholt et al., 2006; Pinker and Ewing, 1985) with MODIS having the advantage of a low SZA during its overflight. These differences in viewing geometry need to be resolved to reconcile differences between sensors. Imagery from ABI also has the potential to estimate the regional decline in vegetation indices after hurricanes (Fig. 5) which can potentially be converted into the decline in GPP using methods described in section 6.1.

6.3 Ecosystem thermodynamics

Observations of the diurnal behavior of land surface attributes can also be used to improve our understanding of the thermal properties of ecosystems. Large-scale changes to ecosystems, such as logging, the conversion of grasslands or forests to farmland, and wildland fires alter the mechanisms by which ecosystems regulate their energy acquisition and heat exchange, thought to be related to the degree of complexity of the system (Kay and Schneider, 1992). The process of ecological succession modifies the structure of an ecosystem over time by gradually increasing its complexity (Odum, 1969). Ecosystems should therefore develop an increasing ability to dissipate incoming solar radiation as succession proceeds (Schneider and Kay, 1994) and, due to a higher order of complex structures, will improve cooling by transferring solar radiation into latent heat and metabolic energy (Norris et al., 2011). Effective energy dissipation results in a cooler surface (with less waste heat) for biological processes to occur. Diurnal patterns of LST can be used to quantify ecological complexity (Lin et al., 2009) and entropy production (Brunsell et al., 2011; Holdaway et al., 2010; Stoy et al., 2014b; Wiesner et al., 2019) and may be useful for monitoring the success of ecological restoration projects that seek to re-establish ecological function (Aerts et al., 2004).

6.4 Satellite data fusion products

One of the most promising applications of geostationary satellites for land surface science may simply be their ability to provide temporally dense observations that can be combined (“fused”) with spatially dense observations from polar-orbiting or other satellite platforms. Such fusion products take advantage of the best features of different platforms, for example by exploiting the finer spatial resolution of observations from Landsat, Sentinel-2, MODIS, VIIRS, or the recently harmonized Landsat Sentinel-2 surface reflectance and the temporal resolution of GOES observations. Based on the assumption that changes in a Landsat pixel are equivalent or proportional to the changes in the co-located MODIS pixel between two dates,

https://doi.org/10.5194/bg-2020-454
Preprint. Discussion started: 8 January 2021

fusion algorithms are able to predict the surface reflectance of a Landsat pixel between acquisition dates using the change observed in MODIS pixels between the reference and prediction date (Gao et al., 2015). Multi-sensor fusion using polar-orbiting and geostationary satellites have provided higher spatiotemporal resolution for estimates of forest disturbance, NDVI, phenology, LST, ET, and water management, yield estimation, and fire radiative power (Cammalleri et al., 2013, 2014; Gao et al., 2015; Hilker et al., 2009; Knauer et al., 2016; Li et al., 2019a; Semmens et al., 2016; Wu et al., 2015; Yang et al., 2018; Zhao and Duan, 2020). Given the importance of considering landscape heterogeneity in using satellite data to estimate various ecosystem variables and model processes such as LUE, carbon flux and storage, phenology, and ET (Ahl et al., 2004; Cammalleri et al., 2014; Leitão et al., 2018; Zeng et al., 2020), multi-sensor data fusion offers a way to address the relatively coarse spatial scale of imagery from geostationary satellites as we expand their use in studying ecosystem function and surface-atmosphere exchange.

7 Conclusions

The recently increased spectral and spatial resolution of imagers onboard geostationary satellites creates new opportunities to use remotely-sensed observations in environmental science, especially when combined with ongoing and forthcoming improvements to the spectral sensitivity of other geostationary imagers. The increased diurnal sampling from ABI can find cloud-free observations when polar-orbiting satellites may be hindered by cloud cover to improve time series of vegetation greenness, canopy water content, LST, and energy-water-carbon fluxes. Temporally-dense geostationary observations have been crucial in detecting moisture stress and wildfires. Extending the use of these observations to measure more land surface variables should result in capturing sudden changes in ecosystem fluxes due to changing atmospheric conditions and extreme events. Furthermore, estimations of vegetation phenological cycles can be improved using geostationary satellites, especially by taking advantage of short periods of clear skies occurring during times of otherwise persistent cloud cover. Studying ecosystem disturbance events should also benefit through increased availability of observations pre- and post-disturbance to estimate burned area and vegetation recovery. Opportunities to study large-scale ecological restoration efforts stem from diurnal LST measurements that can help track the progression of efficiency in energy dissipation that can arise from increasing ecosystem complexity as succession proceeds. Multi-sensor fusion between relatively coarse geostationary satellite observations and observations from platforms with finer spatial resolution offers a way to resolve within-pixel spatial variability in heterogeneous landscapes.

The ongoing efforts to improve the geolocation and radiometric quality of imagery and providing higher level collections of data with surface reflectance, similar to the MODIS or Landsat program, will be a crucial component of using imagery from geostationary sensors. Furthermore, increased collaboration between the National Science Foundation, NASA, and NOAA with increased funding opportunities to pursue research utilizing imagery from geostationary sensors for investigations in the science topics we have detailed here will help realize the potential of these data. Leveraging the high-frequency observations from geostationary sensors for investigations in environmental science where they have been largely untapped will expand the scope of hyper-temporal remote sensing of the environment.

https://doi.org/10.5194/bg-2020-454
Preprint. Discussion started: 8 January 2021

Data and code availability

The GOES-16 ABI Level 2 Cloud and Moisture Imagery (ABI-L2-MCMIPC) used to make the figures is available through https://registry.opendata.aws/noaa-goes/ . The GOES-16 ABI Level 2 Clear Sky Mask (ABI-L2-ACMC) is available through NOAA's Comprehensive Large Array-Data Stewardship System (CLASS). The MODIS (Terra and Aqua) Level 1B Calibrated Radiances-1km (MOD021KM and MYD021KM) were accessed thought the Level-1 Atmosphere Archive & Distribution System (LAADS) Distributed Active Archive Center (DAAC). The code to produce fig. 2 - 5 is available at https://github.com/anmikhan/envirogoes.git

Author contribution

AMK and PCS conceived of the study and all authors contributed to writing the manuscript.

Competing interests

The authors declare that they have no conflict of interest.

Acknowledgements

We thank Timothy J Schmit and Scott Lindstrom for critical insight into the GOES mission, for assistance with data acquisition, and for valuable comments on the manuscript. We also thank David Wood and Dr. Susi Wiesner for valuable comments on the manuscript.

NOAA NESDIS

PCS acknowledges contributions from the U. S. National Science Foundation awards DEB 1552976 and EF 1702029 and the University of Wisconsin – Madison.

References

Aerts, R., Wagendorp, T., November, E., Behailu, M., Deckers, J. and Muys, B.: Ecosystem thermal buffer capacity as an indicator of the restoration status of protected areas in the northern ethiopian highlands, Restoration Ecology, 12(4), 586–596, doi:10.1111/j.1061-2971.2004.00324.x, 2004.

Ahl, D. E., Gower, S. T., Mackay, D. S., Burrows, S. N., Norman, J. M. and Diak, G. R.: Heterogeneity of light use efficiency in a northern Wisconsin forest: implications for modeling net primary production with remote sensing, Remote Sensing of Environment, 93(1–2), 168–178, doi:10.1016/j.rse.2004.07.003, 2004.

Ahn, J.-H., Park, Y.-J., Ryu, J.-H., Lee, B. and Oh, I. S.: Development of atmospheric correction algorithm for Geostationary Ocean Color Imager (GOCI), Ocean Sci. J., 47(3), 247–259, doi:10.1007/s12601-012-0026-2, 2012.

https://doi.org/10.5194/bg-2020-454
Preprint. Discussion started: 8 January 2021

Anderson, M. C., Hain, C., Otkin, J., Zhan, X., Mo, K., Svoboda, M., Wardlow, B. and Pimstein, A.: An Intercomparison of Drought Indicators Based on Thermal Remote Sensing and NLDAS-2 Simulations with U.S. Drought Monitor Classifications, J. Hydrometeor, 14(4), 1035–1056, doi:10.1175/JHM-D-12-0140.1, 2013.

Anderson, M. C., Kustas, W. P., Norman, J. M., Hain, C. R., Mecikalski, J. R., Schultz, L., González-Dugo, M. P., Cammalleri, C., d'Urso, G., Pimstein, A. and Gao, F.: Mapping daily evapotranspiration at field to continental scales using geostationary and polar orbiting satellite imagery, Hydrol. Earth Syst. Sci., 15(1), 223–239, doi:10.5194/hess-15-223-2011, 2011.

Anderson, M. C., Norman, J. M., Mecikalski, J. R., Otkin, J. A. and Kustas, W. P.: A climatological study of evapotranspiration and moisture stress across the continental United States based on thermal remote sensing: 1. Model formulation, J. Geophys. Res., 112(D10), doi:10.1029/2006JD007506, 2007a.

Anderson, M. C., Norman, J. M., Mecikalski, J. R., Otkin, J. A. and Kustas, W. P.: A climatological study of evapotranspiration and moisture stress across the continental United States based on thermal remote sensing: 2. Surface moisture climatology, J. Geophys. Res., 112(D11), doi:10.1029/2006JD007507, 2007b.

Anderson, M. C., Norman, J. M., Meyers, T. P. and Diak, G. R.: An analytical model for estimating canopy transpiration and carbon assimilation fluxes based on canopy light-use efficiency, Agricultural and Forest Meteorology, 101(4), 265–289, doi:10.1016/S0168-1923(99)00170-7, 2000.

Anderson, M. C., Yang, Y., Xue, J., Knipper, K. R., Yang, Y., Gao, F., Hain, C. R., Kustas, W. P., Cawse-Nicholson, K., Hulley, G., Fisher, J. B., Alfieri, J. G., Meyers, T. P., Prueger, J., Baldocchi, D. D. and Rey-Sanchez, C.: Interoperability of ECOSTRESS and Landsat for mapping evapotranspiration time series at sub-field scales, Remote Sensing of Environment, 112189, doi:10.1016/j.rse.2020.112189, 2020.

Anderson, M. C., Zolin, C., Sentelhas, P., Hain, C., Semmens, K., Yilmaz, M. T., Gao, F., Otkin, J. and Tetrault, R.: Assessing correlations of satellite-derived evapotranspiration, precipitation and leaf area index anomalies with yields of major Brazilian crop, Remote Sens Environ, 174, 82–99, 2016.

Anderson, M., Diak, G., Gao, F., Knipper, K., Hain, C., Eichelmann, E., Hemes, K., Baldocchi, D., Kustas, W. and Yang, Y.: Impact of Insolation Data Source on Remote Sensing Retrievals of Evapotranspiration over the California Delta, Remote Sens (Basel), 11(3), 216, doi:10.3390/rs11030216, 2019.

Anderson, M., Norman, J. M., Diak, G. R., Kustas, W. P. and Mecikalski, J. R.: A Two-Source Time-Integrated Model for Estimating Surface Fluxes Using Thermal Infrared Remote Sensing, Remote Sens. Environ., 60(2), 195–216, doi:10.1016/S0034-4257(96)00215-5, 1997.

Aono, Y. and Kazui, K.: Phenological data series of cherry tree flowering in Kyoto, Japan, and its application to reconstruction of springtime temperatures since the 9th century, Int. J. Climatol., 28(7), 905–914, doi:10.1002/joc.1594, 2008.

Badgley, G., Anderegg, L. D. L., Berry, J. A. and Field, C. B.: Terrestrial gross primary production: Using NIRV to scale from site to globe., Glob. Chang. Biol., 25(11), 3731–3740, doi:10.1111/gcb.14729, 2019.

https://doi.org/10.5194/bg-2020-454
Preprint. Discussion started: 8 January 2021

Badgley, G., Field, C. B. and Berry, J. A.: Canopy near-infrared reflectance and terrestrial photosynthesis., Sci. Adv., 3(3), e1602244, doi:10.1126/sciadv.1602244, 2017.

Baldocchi, D. D., Ryu, Y., Dechant, B., Eichelmann, E., Hemes, K., Ma, S., Sanchez, C. R., Shortt, R., Szutu, D., Valach, A., Verfaillie, J., Badgley, G., Zeng, Y. and Berry, J. A.: Outgoing near-infrared radiation from vegetation scales with canopy photosynthesis across a spectrum of function, structure, physiological capacity, and weather, J. Geophys. Res. Biogeosci., 125(7), doi:10.1029/2019JG005534, 2020.

Bauerle, W. L., Oren, R., Way, D. A., Qian, S. S., Stoy, P. C., Thornton, P. E., Bowden, J. D., Hoffman, F. M. and Reynolds, R. F.: Photoperiodic regulation of the seasonal pattern of photosynthetic capacity and the implications for carbon cycling., Proc Natl Acad Sci USA, 109(22), 8612–8617, doi:10.1073/pnas.1119131109, 2012.

Bieliński, T.: A parallax shift effect correction based on cloud height for geostationary satellites and radar observations, Remote Sens (Basel), 12(3), 365, doi:10.3390/rs12030365, 2020.

Bolton, D. K., Coops, N. C., Hermosilla, T., Wulder, M. A. and White, J. C.: Assessing variability in post-fire forest structure along gradients of productivity in the Canadian boreal using multi-source remote sensing, J. Biogeogr., 44(6), 1294–1305, doi:10.1111/jbi.12947, 2017.

Bradley, N. L., Leopold, A. C., Ross, J. and Huffaker, W.: Phenological changes reflect climate change in Wisconsin, Proc. Natl. Acad. Sci. U. S. A., 96(17), 9701–9704, 1999.

Brown, T. B., Hultine, K. R., Steltzer, H., Denny, E. G., Denslow, M. W., Granados, J., Henderson, S., Moore, D., Nagai, S., SanClements, M., Sánchez-Azofeifa, A., Sonnentag, O., Tazik, D. and Richardson, A. D.: Using phenocams to monitor our changing Earth: toward a global phenocam network, Front. Ecol. Environ., 14(2), 84–93, doi:10.1002/fee.1222, 2016.

Brunsell, N. A., Schymanski, S. J. and Kleidon, A.: Quantifying the thermodynamic entropy budget of the land surface: is this useful?, Earth Syst. Dynam., 2(1), 87–103, doi:10.5194/esd-2-87-2011, 2011.

Cammalleri, C., Anderson, M. C., Gao, F., Hain, C. R. and Kustas, W. P.: A data fusion approach for mapping daily evapotranspiration at field scale, Water Resour. Res., 49(8), 4672–4686, doi:10.1002/wrcr.20349, 2013.

Cammalleri, C., Anderson, M. C., Gao, F., Hain, C. R. and Kustas, W. P.: Mapping daily evapotranspiration at field scales over rainfed and irrigated agricultural areas using remote sensing data fusion, Agricultural and Forest Meteorology, 186, 1–11, doi:10.1016/j.agrformet.2013.11.001, 2014.

Carrer, D., Ceamanos, X., Moparthy, S., Vincent, C., C. Freitas, S. and Trigo, I. F.: Satellite Retrieval of Downwelling Shortwave Surface Flux and Diffuse Fraction under All Sky Conditions in the Framework of the LSA SAF Program (Part 1: Methodology), Remote Sens (Basel), 11(21), 2532, doi:10.3390/rs11212532, 2019.

Chambers, J. Q., Fisher, J. I., Zeng, H., Chapman, E. L., Baker, D. B. and Hurtt, G. C.: Hurricane Katrina's carbon footprint on U.S. Gulf Coast forests., Science, 318(5853), 1107, doi:10.1126/science.1148913, 2007.

Chen, D., Huang, J. and Jackson, T. J.: Vegetation water content estimation for corn and soybeans using spectral indices derived from MODIS near- and short-wave infrared bands, Remote Sensing of Environment, 98(2–3), 225–236, doi:10.1016/j.rse.2005.07.008, 2005.

605 Choi, J.-K., Min, J.-E., Noh, J. H., Han, T.-H., Yoon, S., Park, Y. J., Moon, J.-E., Ahn, J.-H., Ahn, S. M. and Park, J.-H.: Harmful algal bloom (HAB) in the East Sea identified by the Geostationary Ocean Color Imager (GOCI), Harmful Algae, 39, 295–302, doi:10.1016/j.hal.2014.08.010, 2014.

Choi, J.-K., Park, Y. J., Ahn, J. H., Lim, H.-S., Eom, J. and Ryu, J.-H.: GOCI, the world's first geostationary ocean color observation satellite, for the monitoring of temporal variability in coastal water turbidity, J. Geophys. Res., 117(C9),
610 doi:10.1029/2012JC008046, 2012.

Chudnovsky, A., Ben-Dor, E. and Saaroni, H.: Diurnal thermal behavior of selected urban objects using remote sensing measurements, Energy and Buildings, 36(11), 1063–1074, doi:10.1016/j.enbuild.2004.01.052, 2004.

Concha, J., Mannino, A., Franz, B. and Kim, W.: Assessing diurnal variability of biogeochemical processes using the geostationary ocean color imager (GOCI), , doi:10.20944/preprints201811.0042.v1, 2018.

615 Coyle, D. B., Stysley, P. R., Poulios, D., Clarke, G. B. and Kay, R. B.: Laser transmitter development for NASA's Global Ecosystem Dynamics Investigation (GEDI) lidar, in Lidar Remote Sensing for Environmental Monitoring XV, vol. 9612, edited by U. N. Singh, p. 961208, SPIE., 2015.

Dannenberg, M., Wang, X., Yan, D. and Smith, W.: Phenological characteristics of global ecosystems based on optical, fluorescence, and microwave remote sensing, Remote Sens (Basel), 12(4), 671, doi:10.3390/rs12040671, 2020.

620 De Araujo Barbosa, C. C., Atkinson, P. M. and Dearing, J. A.: Remote sensing of ecosystem services: A systematic review, Ecological Indicators, 52(52), 430–443, doi:10.1016/j.ecolind.2015.01.007, 2015.

Diak, G. R.: Investigations of improvements to an operational GOES-satellite-data-based insolation system using pyranometer data from the U.S. Climate Reference Network (USCRN), Remote Sensing of Environment, 195, 79–95, doi:10.1016/j.rse.2017.04.002, 2017.

625 Diak, G. R. and Gautier, C.: Improvements to a Simple Physical Model for Estimating Insolation from GOES Data, J. Climate Appl. Meteor., 22(3), 505–508, doi:10.1175/1520-0450(1983)022<0505:ITASPM>2.0.CO;2, 1983.

Diak, G. R. and Stewart, T. R.: Assessment of surface turbulent fluxes using geostationary satellite surface skin temperatures and a mixed layer planetary boundary layer scheme, J. Geophys. Res., 94(D5), 6357, doi:10.1029/JD094iD05p06357, 1989.

Diak, G. R. and Whipple, M. S.: Note on estimating surface sensible heat fluxes using surface temperatures measured from a
630 geostationary satellite during FIFE 1989, J. Geophys. Res., 100(D12), 25453, doi:10.1029/95JD00729, 1995.

DOC, NOAA, NESDIS, NASA: Product Definition and User's Guide (PUG): Volume 3: Level 1b Products, [online] Available from: https://www.goes-r.gov/users/docs/PUG-L1b-vol3.pdf (Accessed 8 August 2020), 2019.

Dutkiewicz, S., Hickman, A. E., Jahn, O., Henson, S., Beaulieu, C. and Monier, E.: Ocean colour signature of climate change., Nat. Commun., 10(1), 578, doi:10.1038/s41467-019-08457-x, 2019.

635 Emmel, C., D'Odorico, P., Revill, A., Hörtnagl, L., Ammann, C., Buchmann, N. and Eugster, W.: Canopy photosynthesis of six major arable crops is enhanced under diffuse light due to canopy architecture., Glob. Chang. Biol., doi:10.1111/gcb.15226, 2020.

https://doi.org/10.5194/bg-2020-454
Preprint. Discussion started: 8 January 2021

Erbs, D. G., Klein, S. A. and Duffie, J. A.: Estimation of the diffuse radiation fraction for hourly, daily and monthly-average global radiation, Solar Energy, 28(4), 293–302, doi:10.1016/0038-092X(82)90302-4, 1982.

Fang, L., Zhan, X., Schull, M., Kalluri, S., Laszlo, I., Yu, P., Carter, C., Hain, C. and Anderson, M.: Evapotranspiration Data Product from NESDIS GET-D System Upgraded for GOES-16 ABI Observations, Remote Sens (Basel), 11(22), 2639, doi:10.3390/rs11222639, 2019.

Fensholt, R. and Sandholt, I.: Derivation of a shortwave infrared water stress index from MODIS near- and shortwave infrared data in a semiarid environment, Remote Sensing of Environment, 87(1), 111–121, doi:10.1016/j.rse.2003.07.002, 2003.

Fensholt, R., Sandholt, I., Stisen, S. and Tucker, C.: Analysing NDVI for the African continent using the geostationary meteosat second generation SEVIRI sensor, Remote Sensing of Environment, 101(2), 212–229, doi:10.1016/j.rse.2005.11.013, 2006.

Filippa, G., Cremonese, E., Migliavacca, M., Galvagno, M., Sonnentag, O., Humphreys, E., Hufkens, K., Ryu, Y., Verfaillie, J., Morra di Cella, U. and Richardson, A. D.: NDVI derived from near-infrared-enabled digital cameras: Applicability across different plant functional types, Agricultural and Forest Meteorology, 249, 275–285, doi:10.1016/j.agrformet.2017.11.003, 2018.

Fu, Z., Stoy, P. C., Luo, Y., Chen, J., Sun, J., Montagnani, L., Wohlfahrt, G., Rahman, A. F., Rambal, S., Bernhofer, C., Wang, J., Shirkey, G. and Niu, S.: Climate controls over the net carbon uptake period and amplitude of net ecosystem production in temperate and boreal ecosystems, Agricultural and Forest Meteorology, 243, 9–18, doi:10.1016/j.agrformet.2017.05.009, 2017.

Fu, Z., Stoy, P. C., Poulter, B., Gerken, T., Zhang, Z., Wakbulcho, G. and Niu, S.: Maximum carbon uptake rate dominates the interannual variability of global net ecosystem exchange., Glob. Chang. Biol., 25(10), 3381–3394, doi:10.1111/gcb.14731, 2019.

Gamon, J. A., Field, C. B., Goulden, M. L., Griffin, K. L., Hartley, A. E., Joel, G., Penuelas, J. and Valentini, R.: Relationships between NDVI, canopy structure, and photosynthesis in three californian vegetation types, Ecol. Appl., 5(1), 28–41, doi:10.2307/1942049, 1995.

Gamon, J. A., Huemmrich, K. F., Wong, C. Y. S., Ensminger, I., Garrity, S., Hollinger, D. Y., Noormets, A. and Peñuelas, J.: A remotely sensed pigment index reveals photosynthetic phenology in evergreen conifers., Proc Natl Acad Sci USA, 113(46), 13087–13092, doi:10.1073/pnas.1606162113, 2016.

Ganguly, S., Friedl, M. A., Tan, B., Zhang, X. and Verma, M.: Land surface phenology from MODIS: Characterization of the Collection 5 global land cover dynamics product, Remote Sensing of Environment, 114(8), 1805–1816, doi:10.1016/j.rse.2010.04.005, 2010.

Gao, B.: NDWI—A normalized difference water index for remote sensing of vegetation liquid water from space, Remote Sensing of Environment, 58(3), 257–266, doi:10.1016/S0034-4257(96)00067-3, 1996.

Gao, F., Hilker, T., Zhu, X., Anderson, M., Masek, J., Wang, P. and Yang, Y.: Fusing landsat and MODIS data for vegetation monitoring, IEEE Geosci. Remote Sens. Mag., 3(3), 47–60, doi:10.1109/MGRS.2015.2434351, 2015.

García-Haro, F. J., Campos-Taberner, M., Moreno, Á., Tagesson, H. T., Camacho, F., Martínez, B., Sánchez, S., Piles, M., Camps-Valls, G., Yebra, M. and Gilabert, M. A.: A global canopy water content product from AVHRR/Metop, ISPRS Journal of Photogrammetry and Remote Sensing, 162, 77–93, doi:10.1016/j.isprsjprs.2020.02.007, 2020.

Gautier, C., Diak, G. and Masse, S.: A Simple Physical Model to Estimate Incident Solar Radiation at the Surface from GOES Satellite Data, J. Appl. Meteor., 19(8), 1005–1012, doi:10.1175/1520-0450(1980)019<1005:ASPMTE>2.0.CO;2, 1980.

Ghilain, N., Arboleda, A. and Gellens-Meulenberghs, F.: Evapotranspiration modelling at large scale using near-real time MSG SEVIRI derived data, Hydrol. Earth Syst. Sci., 15(3), 771–786, doi:10.5194/hess-15-771-2011, 2011.

Goetz, S. J., Fiske, G. J. and Bunn, A. G.: Using satellite time-series data sets to analyze fire disturbance and forest recovery across Canada, Remote Sensing of Environment, 101(3), 352–365, doi:10.1016/j.rse.2006.01.011, 2006.

Good, E.: Daily minimum and maximum surface air temperatures from geostationary satellite data, J. Geophys. Res. Atmos., 120(6), 2306–2324, doi:10.1002/2014JD022438, 2015.

Govaerts, Y. M., Wagner, S., Lattanzio, A. and Watts, P.: Joint retrieval of surface reflectance and aerosol optical depth from MSG/SEVIRI observations with an optimal estimation approach: 1. Theory, J. Geophys. Res., 115(D2), doi:10.1029/2009JD011779, 2010.

Grant, I. F., Prata, A. J. and Cechet, R. P.: The impact of the diurnal variation of albedo on the remote sensing of the daily mean albedo of grassland, J. Appl. Meteor., 39(2), 231–244, doi:10.1175/1520-0450(2000)039<0231:TIOTDV>2.0.CO;2, 2000.

Guan, K., Medvigy, D., Wood, E. F., Caylor, K. K., Li, S. and Jeong, S.-J.: Deriving vegetation phenological time and trajectory information over africa using SEVIRI daily LAI, IEEE Trans. Geosci. Remote Sensing, 52(2), 1113–1130, doi:10.1109/TGRS.2013.2247611, 2014.

Gu, L., Baldocchi, D. D., Wofsy, S. C., Munger, J. W., Michalsky, J. J., Urbanski, S. P. and Boden, T. A.: Response of a deciduous forest to the Mount Pinatubo eruption: enhanced photosynthesis., Science, 299(5615), 2035–2038, doi:10.1126/science.1078366, 2003.

Hardisky, M. A., Klemas, V. and Smart, R. M.: The Influence of Soil Salinity, Growth Form, and Leaf Moisture on the Spectral Radiance of Spartina alterniflora Canopies, Photogrammetric Engineering & Remote Sensing, 49(1), 77–83, 1983.

Hemes, K. S., Verfaillie, J. and Baldocchi, D. D.: Wildfire-smoke aerosols lead to increased light use efficiency among agricultural and restored wetland land uses in california's central valley, J. Geophys. Res. Biogeosci., 125(2), doi:10.1029/2019JG005380, 2020.

He, T., Liang, S., Wang, D., Wu, H., Yu, Y. and Wang, J.: Estimation of surface albedo and directional reflectance from Moderate Resolution Imaging Spectroradiometer (MODIS) observations, Remote Sensing of Environment, 119, 286–300, doi:10.1016/j.rse.2012.01.004, 2012.

He, Zhang, Liang, Yu and Wang: Developing Land Surface Directional Reflectance and Albedo Products from Geostationary GOES-R and Himawari Data: Theoretical Basis, Operational Implementation, and Validation, Remote Sens (Basel), 11(22), 2655, doi:10.3390/rs11222655, 2019.

Hilker, T., Wulder, M. A., Coops, N. C., Linke, J., McDermid, G., Masek, J. G., Gao, F. and White, J. C.: A new data fusion model for high spatial- and temporal-resolution mapping of forest disturbance based on Landsat and MODIS, Remote Sensing of Environment, 113(8), 1613–1627, doi:10.1016/j.rse.2009.03.007, 2009.

Holdaway, R. J., Sparrow, A. D. and Coomes, D. A.: Trends in entropy production during ecosystem development in the Amazon Basin., Philos. Trans. R. Soc. Lond. B. Biol. Sci, 365(1545), 1437–1447, doi:10.1098/rstb.2009.0298, 2010.

Huete, A., Didan, K., Miura, T., Rodriguez, E. P., Gao, X. and Ferreira, L. G.: Overview of the radiometric and biophysical performance of the MODIS vegetation indices, Remote Sensing of Environment, 83(1–2), 195–213, doi:10.1016/S0034-4257(02)00096-2, 2002.

Hulley, G., Hook, S., Fisher, J. and Lee, C.: ECOSTRESS, A NASA Earth-Ventures Instrument for studying links between the water cycle and plant health over the diurnal cycle, in 2017 IEEE International Geoscience and Remote Sensing Symposium (IGARSS), pp. 5494–5496, IEEE., 2017.

Jackson, T. J., Chen, D., Cosh, M., Li, F., Anderson, M., Walthall, C., Doriaswamy, P. and Hunt, E. R.: Vegetation water content mapping using Landsat data derived normalized difference water index for corn and soybeans, Remote Sensing of Environment, 92(4), 475–482, doi:10.1016/j.rse.2003.10.021, 2004.

Janjai, S. and Wattan, R.: Development of a model for the estimation of photosynthetically active radiation from geostationary satellite data in a tropical environment, Remote Sensing of Environment, 115(7), 1680–1693, doi:10.1016/j.rse.2011.02.026, 2011.

Jarvis, P. G.: The Interpretation of the Variations in Leaf Water Potential and Stomatal Conductance Found in Canopies in the Field, Philosophical Transactions of the Royal Society B: Biological Sciences, 273(927), 593–610, doi:10.1098/rstb.1976.0035, 1976.

Jolliff, J. K., Lewis, M. D., Ladner, S. and Crout, R. L.: Observing the Ocean Submesoscale with Enhanced-Color GOES-ABI Visible Band Data., Sensors, 19(18), doi:10.3390/s19183900, 2019.

Jordan, C. F.: Derivation of Leaf-Area Index from Quality of Light on the Forest Floor, Ecology, 50(4), 663, doi:10.2307/1936256, 1969.

Kannenberg, S. A., Bowling, D. R. and Anderegg, W. R. L.: Hot moments in ecosystem fluxes: High GPP anomalies exert outsized influence on the carbon cycle and are differentially driven by moisture availability across biomes, Environmental Research Letters, 15(5), 054004, doi:10.1088/1748-9326/ab7b97, 2020.

Kay, J. J. and Schneider, E. D.: Thermodynamics and measures of ecological integrity, in Ecological Indicators, edited by D. H. McKenzie, D. E. Hyatt, and V. J. McDonald, pp. 159–182, Springer US, Boston, MA., 1992.

Kerr, J. T. and Ostrovsky, M.: From space to species: ecological applications for remote sensing, Trends Ecol Evol (Amst), 18(6), 299–305, doi:10.1016/S0169-5347(03)00071-5, 2003.

Kim, H.-W., Yeom, J.-M., Shin, D., Choi, S., Han, K.-S. and Roujean, J.-L.: An assessment of thin cloud detection by applying bidirectional reflectance distribution function model-based background surface reflectance using Geostationary Ocean Color Imager (GOCI): A case study for South Korea, J. Geophys. Res. Atmos., 122(15), 8153–8172, doi:10.1002/2017JD026707, 2017.

Knauer, K., Gessner, U., Fensholt, R. and Kuenzer, C.: An ESTARFM Fusion Framework for the Generation of Large-Scale Time Series in Cloud-Prone and Heterogeneous Landscapes, Remote Sens (Basel), 8(5), 425, doi:10.3390/rs8050425, 2016.

LeBauer, D., Wang, D., Feng, X. and Dietze, M.: PECAn: workflow management for data assimilation and forecasting, Nature Precedings, doi:10.1038/npre.2011.5533.1, 2011.

Leitão, P. J., Schwieder, M., Pötzschner, F., Pinto, J. R. R., Teixeira, A. M. C., Pedroni, F., Sanchez, M., Rogass, C., van der Linden, S., Bustamante, M. M. C. and Hostert, P.: From sample to pixel: multi-scale remote sensing data for upscaling aboveground carbon data in heterogeneous landscapes, Ecosphere, 9(8), e02298, doi:10.1002/ecs2.2298, 2018.

Lin, H., Cao, M., Stoy, P. C. and Zhang, Y.: Assessing self-organization of plant communities—A thermodynamic approach, Ecol. Modell., 220(6), 784–790, doi:10.1016/j.ecolmodel.2009.01.003, 2009.

Liu, Y., Hill, M. J., Zhang, X., Wang, Z., Richardson, A. D., Hufkens, K., Filippa, G., Baldocchi, D. D., Ma, S., Verfaillie, J. and Schaaf, C. B.: Using data from Landsat, MODIS, VIIRS and PhenoCams to monitor the phenology of California oak/grass savanna and open grassland across spatial scales, Agricultural and Forest Meteorology, 237–238, 311–325, doi:10.1016/j.agrformet.2017.02.026, 2017.

Li, F., Zhang, X., Roy, D. P. and Kondragunta, S.: Estimation of biomass-burning emissions by fusing the fire radiative power retrievals from polar-orbiting and geostationary satellites across the conterminous United States, Atmos. Environ., 211, 274–287, doi:10.1016/j.atmosenv.2019.05.017, 2019a.

Li, S., Wang, W., Hashimoto, H., Xiong, J., Vandal, T., Yao, J., Qian, L., Ichii, K., Lyapustin, A., Wang, Y. and Nemani, R.: First Provisional Land Surface Reflectance Product from Geostationary Satellite Himawari-8 AHI, Remote Sens (Basel), 11(24), 2990, doi:10.3390/rs11242990, 2019b.

Li, Z.-L., Tang, B.-H., Wu, H., Ren, H., Yan, G., Wan, Z., Trigo, I. F. and Sobrino, J. A.: Satellite-derived land surface temperature: Current status and perspectives, Remote Sensing of Environment, 131, 14–37, doi:10.1016/j.rse.2012.12.008, 2013.

Mahadevan, P., Wofsy, S. C., Matross, D. M., Xiao, X., Dunn, A. L., Lin, J. C., Gerbig, C., Munger, J. W., Chow, V. Y. and Gottlieb, E. W.: A satellite-based biosphere parameterization for net ecosystem CO2 exchange: Vegetation Photosynthesis and Respiration Model (VPRM), Global Biogeochem. Cycles, 22(2), doi:10.1029/2006GB002735, 2008.

Ma, X., Huete, A., Tran, N. N., Bi, J., Gao, S. and Zeng, Y.: Sun-Angle Effects on Remote-Sensing Phenology Observed and Modelled Using Himawari-8, Remote Sens (Basel), 12(8), 1339, doi:10.3390/rs12081339, 2020.

McCallum, I., Wagner, W., Schmullius, C., Shvidenko, A., Obersteiner, M., Fritz, S. and Nilsson, S.: Satellite-based terrestrial production efficiency modeling., Carbon Balance Manag., 4, 8, doi:10.1186/1750-0680-4-8, 2009.

McCorkel, J., Efremova, B., Hair, J., Andrade, M. and Holben, B.: GOES-16 ABI solar reflective channel validation for earth science application, Remote Sensing of Environment, 237, 111438, doi:10.1016/j.rse.2019.111438, 2020.

Mecikalski, J. R., Diak, G. R., Anderson, M. C. and Norman, J. M.: Estimating fluxes on continental scales using remotely sensed data in an atmospheric–land exchange model, J. Appl. Meteor., 38(9), 1352–1369, doi:10.1175/1520-0450(1999)038<1352:EFOCSU>2.0.CO;2, 1999.

Meng, R., Wu, J., Zhao, F., Cook, B. D., Hanavan, R. P. and Serbin, S. P.: Measuring short-term post-fire forest recovery across a burn severity gradient in a mixed pine-oak forest using multi-sensor remote sensing techniques, Remote Sensing of Environment, 210, 282–296, doi:10.1016/j.rse.2018.03.019, 2018.

Menzel, W. P.: History of geostationary weather satellites, in The GOES-R Series, pp. 5–11, Elsevier., 2020.

Mercado, L. M., Bellouin, N., Sitch, S., Boucher, O., Huntingford, C., Wild, M. and Cox, P. M.: Impact of changes in diffuse radiation on the global land carbon sink., Nature, 458(7241), 1014–1017, doi:10.1038/nature07949, 2009.

Miura, T., Nagai, S., Takeuchi, M., Ichii, K. and Yoshioka, H.: Improved Characterisation of Vegetation and Land Surface Seasonal Dynamics in Central Japan with Himawari-8 Hypertemporal Data., Sci. Rep., 9(1), 15692, doi:10.1038/s41598-019-52076-x, 2019.

Monteith, J. L.: Solar radiation and productivity in tropical ecosystems, J. Appl. Ecol., 9(3), 747, doi:10.2307/2401901, 1972.

Neukermans, G., Ruddick, K., Bernard, E., Ramon, D., Nechad, B. and Deschamps, P.-Y.: Mapping total suspended matter from geostationary satellites: a feasibility study with SEVIRI in the Southern North Sea, Opt. Express, 17(16), 14029–14052, 2009.

Nieke, J., Borde, F., Mavrocordatos, C., Berruti, B., Delclaud, Y., Riti, J. B. and Garnier, T.: The Ocean and Land Colour Imager (OLCI) for the Sentinel 3 GMES Mission: status and first test results, in Earth Observing Missions and Sensors: Development, Implementation, and Characterization II, vol. 8528, edited by H. Shimoda, X. Xiong, C. Cao, X. Gu, C. Kim, and A. S. Kiran Kumar, p. 85280C, SPIE., 2012.

NOAA: Summary of the GOES-17 Cooling System Issue, GOES Image Viewer [online] Available from: https://www.star.nesdis.noaa.gov/GOES/loopheatpipeanomaly.php (Accessed 29 October 2020), n.d.

NOAA and NASA: GOES-17 ABI Performance, GOES-R [online] Available from: https://www.goes-r.gov/users/GOES-17-ABI-Performance.html (Accessed 4 November 2020), n.d.

Noh, J. H., Kim, W., Son, S. H., Ahn, J.-H. and Park, Y.-J.: Remote quantification of Cochlodinium polykrikoides blooms occurring in the East Sea using geostationary ocean color imager (GOCI)., Harmful Algae, 73, 129–137, doi:10.1016/j.hal.2018.02.006, 2018.

Norman, J. M., Kustas, W. P. and Humes, K. S.: Source approach for estimating soil and vegetation energy fluxes in observations of directional radiometric surface temperature, Agricultural and Forest Meteorology, 77(3–4), 263–293, doi:10.1016/0168-1923(95)02265-Y, 1995.

Odum, E. P.: The Strategy of Ecosystem Development, Science, 164(3877), 262–270, doi:10.1126/science.164.3877.262, 1969.

Oliphant, A. J. and Stoy, P. C.: An evaluation of semiempirical models for partitioning photosynthetically active radiation into diffuse and direct beam components, J. Geophys. Res. Biogeosci., 123(3), 889–901, doi:10.1002/2017JG004370, 2018.

Otkin, J. A., Anderson, M. C., Hain, C., Mladenova, I. E., Basara, J. B. and Svoboda, M.: Examining rapid onset drought development using the thermal infrared–based evaporative stress index, J. Hydrometeor, 14(4), 1057–1074, doi:10.1175/JHM-D-12-0144.1, 2013.

Otkin, J. A., Anderson, M. C., Hain, C. and Svoboda, M.: Examining the Relationship between Drought Development and Rapid Changes in the Evaporative Stress Index, J. Hydrometeor, 15(3), 938–956, doi:10.1175/JHM-D-13-0110.1, 2014.

Otkin, J. A., Anderson, M. C., Hain, C., Svoboda, M., Johnson, D., Mueller, R., Tadesse, T., Wardlow, B. and Brown, J.: Assessing the evolution of soil moisture and vegetation conditions during the 2012 United States flash drought, Agricultural and Forest Meteorology, 218–219, 230–242, doi:10.1016/j.agrformet.2015.12.065, 2016.

Otkin, J. A., Anderson, M. C., Mecikalski, J. R. and Diak, G. R.: Validation of GOES-Based Insolation Estimates Using Data from the U.S. Climate Reference Network, J. Hydrometeor, 6(4), 460–475, doi:10.1175/JHM440.1, 2005.

Otkin, J. A., Haigh, T., Mucia, A., Anderson, M. C. and Hain, C.: Comparison of Agricultural Stakeholder Survey Results and Drought Monitoring Datasets during the 2016 U.S. Northern Plains Flash Drought, Wea. Climate Soc., 10(4), 867–883, doi:10.1175/WCAS-D-18-0051.1, 2018a.

Otkin, J. A., Shafer, M., Svoboda, M., Wardlow, B., Anderson, M. C., Hain, C. and Basara, J.: Facilitating the Use of Drought Early Warning Information through Interactions with Agricultural Stakeholders, Bull. Amer. Meteor. Soc., 96(7), 1073–1078, doi:10.1175/BAMS-D-14-00219.1, 2015.

Otkin, J. A., Svoboda, M., Hunt, E. D., Ford, T. W., Anderson, M. C., Hain, C. and Basara, J. B.: Flash droughts: a review and assessment of the challenges imposed by rapid onset droughts in the united states, Bull. Amer. Meteor. Soc., 99(5), 911–915, doi:10.1175/BAMS-D-17-0149.1, 2018b.

Ouaknine, J., Gode, S., Napierala, B., Viard, T., Foerster, U., Fray, S., Peacoke, P., Hartl, M., Hallibert, P. and Durand, Y.: MTG Flexible Combined Imager optical design and performances, in Earth Observing Systems XVIII, vol. 8866, edited by J. J. Butler, X. (Jack) Xiong, and X. Gu, p. 88661A, SPIE., 2013.

Park, K.-A., Woo, H.-J. and Ryu, J.-H.: Spatial scales of mesoscale eddies from GOCI Chlorophyll-a concentration images in the East/Japan Sea, Ocean Sci. J., 47(3), 347–358, doi:10.1007/s12601-012-0033-3, 2012.

Peres, L. F. and DaCamara, C. C.: Emissivity maps to retrieve land-surface temperature from MSG/SEVIRI, IEEE Trans. Geosci. Remote Sensing, 43(8), 1834–1844, doi:10.1109/TGRS.2005.851172, 2005.

Peschoud, C., Minghelli, A., Mathieu, S., Lei, M., Pairaud, I. and Pinazo, C.: Fusion of Sun-Synchronous and Geostationary Images for Coastal and Ocean Color Survey Application to OLCI (Sentinel-3) and FCI (MTG), IEEE J. Sel. Top. Appl. Earth Observations Remote Sensing, 10(1), 45–56, doi:10.1109/JSTARS.2016.2558819, 2017.

Piao, S., Liu, Q., Chen, A., Janssens, I. A., Fu, Y., Dai, J., Liu, L., Lian, X., Shen, M. and Zhu, X.: Plant phenology and global climate change: Current progresses and challenges., Glob. Chang. Biol., 25(6), 1922–1940, doi:10.1111/gcb.14619, 2019.

Pinker, R. T. and Ewing, J. A.: Modeling surface solar radiation: model formulation and validation, J. Climate Appl. Meteor., 24(5), 389–401, doi:10.1175/1520-0450(1985)024<0389:MSSRMF>2.0.CO;2, 1985.

Pinker, R. T., Laszlo, I., Tarpley, J. D. and Mitchell, K.: Geostationary satellite parameters for surface energy balance, Adv. Space Res., 30(11), 2427–2432, doi:10.1016/S0273-1177(02)80296-4, 2002.

Pinker, R. T., Ma, Y., Chen, W., Hulley, G., Borbas, E., Islam, T., Hain, C., Cawse-Nicholson, K., Hook, S. and Basara, J.: Towards a Unified and Coherent Land Surface Temperature Earth System Data Record from Geostationary Satellites, Remote Sens (Basel), 11(12), 1399, doi:10.3390/rs11121399, 2019.

Prins, E. M. and Menzel, W. P.: Trends in South American biomass burning detected with the GOES visible infrared spin scan radiometer atmospheric sounder from 1983 to 1991, J. Geophys. Res., 99(D8), 16719, doi:10.1029/94JD01208, 1994.

Qi, W., Lee, S.-K., Hancock, S., Luthcke, S., Tang, H., Armston, J. and Dubayah, R.: Improved forest height estimation by fusion of simulated GEDI Lidar data and TanDEM-X InSAR data, Remote Sensing of Environment, 221, 621–634, doi:10.1016/j.rse.2018.11.035, 2019.

Randazzo, N. A., Michalak, A. M. and Desai, A. R.: Synoptic meteorology explains temperate forest carbon uptake, J. Geophys. Res. Biogeosci., doi:10.1029/2019JG005476, 2020.

Richardson, A. D., Keenan, T. F., Migliavacca, M., Ryu, Y., Sonnentag, O. and Toomey, M.: Climate change, phenology, and phenological control of vegetation feedbacks to the climate system, Agricultural and Forest Meteorology, 169, 156–173, doi:10.1016/j.agrformet.2012.09.012, 2013.

Robinson, N. P., Allred, B. W., Smith, W. K., Jones, M. O., Moreno, A., Erickson, T. A., Naugle, D. E. and Running, S. W.: Terrestrial primary production for the conterminous United States derived from Landsat 30 m and MODIS 250 m, Remote Sens. Ecol. Conserv., doi:10.1002/rse2.74, 2018.

Roujean, J.-L. and Lacaze, R.: Global mapping of vegetation parameters from POLDER multiangular measurements for studies of surface-atmosphere interactions: A pragmatic method and its validation, J. Geophys. Res., 107(D12), 4150, doi:10.1029/2001JD000751, 2002.

Rouse, J. W., Haas, R. H. J., Schell, J. A. and Deering, D. W.: MONITORING VEGETATION SYSTEMS IN THE GREAT PLAINS WITH ERTS, in Third Earth Resource Technology Satellite - 1 Symposium, vol. 1, edited by S. C. Freden, E. P. Mercanti, and M. A. Becker, pp. 309–317, NASA Scientific and Technical Information Office. [online] Available from: https://ntrs.nasa.gov/archive/nasa/casi.ntrs.nasa.gov/19740022614.pdf (Accessed 15 May 2020), 1974.

Ruddick, K., Neukermans, G., Vanhellemont, Q. and Jolivet, D.: Challenges and opportunities for geostationary ocean colour remote sensing of regional seas: A review of recent results, Remote Sensing of Environment, 146, 63–76, doi:10.1016/j.rse.2013.07.039, 2014.

Running, S. W., Nemani, R. R., Heinsch, F. A., Zhao, M., Reeves, M. and Hashimoto, H.: A Continuous Satellite-Derived Measure of Global Terrestrial Primary Production, Bioscience, 54(6), 547, doi:10.1641/0006-3568(2004)054[0547:ACSMOG]2.0.CO;2, 2004.

Running, S. W., Peterson, D. L., Spanner, M. A. and Teuber, K. B.: Remote sensing of coniferous forest leaf area, Ecology, 67(1), 273–276, doi:10.2307/1938532, 1986.

Ryu, J.-H., Han, H.-J., Cho, S., Park, Y.-J. and Ahn, Y.-H.: Overview of geostationary ocean color imager (GOCI) and GOCI data processing system (GDPS), Ocean Sci. J., 47(3), 223–233, doi:10.1007/s12601-012-0024-4, 2012.

Ryu, J.-H. and Ishizaka, J.: GOCI data processing and ocean applications, Ocean Sci. J., 47(3), 221–221, doi:10.1007/s12601-012-0023-5, 2012.

S. Ha, W., R. Diak, G. and F. Krajewski, W.: Estimating Near Real-Time Hourly Evapotranspiration Using Numerical Weather Prediction Model Output and GOES Remote Sensing Data in Iowa, Remote Sens (Basel), 12(14), 2337, doi:10.3390/rs12142337, 2020.

Schmetz, J., Pili, P., Tjemkes, S., Just, D., Kerkmann, J., Rota, S. and Ratier, A.: An introduction to meteosat second generation (MSG), Bull. Amer. Meteor. Soc., 83(7), 977–992, doi:10.1175/1520-0477(2002)083<0977:AITMSG>2.3.CO;2, 2002.

Schmidt, C. C., Hoffman, J., Prins, E. and Lindstrom, S.: GOES-R Advanced Baseline Imager (ABI) Algorithm Theoretical Basis Document For Fire / Hot Spot Characterization, NOAA NESDIS CENTER for SATELLITE APPLICATIONS and RESEARCH., 2012.

Schmit, T. J., Goodman, S. J., Gunshor, M. M., Sieglaff, J., Heidinger, A. K., Bachmeier, A. S., Lindstrom, S. S., Terborg, A., Feltz, J., Bah, K., Rudlosky, S., Lindsey, D. T., Rabin, R. M. and Schmidt, C. C.: Rapid refresh information of significant events: preparing users for the next generation of geostationary operational satellites, Bull. Amer. Meteor. Soc., 96(4), 561–576, doi:10.1175/BAMS-D-13-00210.1, 2015.

Schmit, T. J., Griffith, P., Gunshor, M. M., Daniels, J. M., Goodman, S. J. and Lebair, W. J.: A Closer Look at the ABI on the GOES-R Series, Bull. Amer. Meteor. Soc., 98(4), 681–698, doi:10.1175/BAMS-D-15-00230.1, 2017.

Schmit, T. J. and Gunshor, M. M.: ABI Imagery from the GOES-R Series, in The GOES-R Series, pp. 23–34, Elsevier., 2020.

Schmit, T. J., Lindstrom, S. S., Gerth, J. J. and Gunshor, M. M.: Applications of the 16 spectral bands on the Advanced Baseline Imager (ABI)., J. Operational Meteor., 06(04), 33–46, doi:10.15191/nwajom.2018.0604, 2018.

Schumacher, D. L., Keune, J. and Miralles, D. G.: Atmospheric heat and moisture transport to energy- and water-limited ecosystems., Ann. N. Y. Acad. Sci., doi:10.1111/nyas.14357, 2020.

Semmens, K. A., Anderson, M. C., Kustas, W. P., Gao, F., Alfieri, J. G., McKee, L., Prueger, J. H., Hain, C. R., Cammalleri, C., Yang, Y., Xia, T., Sanchez, L., Mar Alsina, M. and Vélez, M.: Monitoring daily evapotranspiration over two California vineyards using Landsat 8 in a multi-sensor data fusion approach, Remote Sensing of Environment, 185, 155–170, doi:10.1016/j.rse.2015.10.025, 2016.

905 Seong, N.-H., Jung, D., Kim, J. and Han, K.-S.: Evaluation of NDVI Estimation Considering Atmospheric and BRDF Correction through Himawari-8/AHI, Asia-Pacific J Atmos Sci, 56(2), 265–274, doi:10.1007/s13143-019-00167-0, 2020.

Seyednasrollah, B., Young, A. M., Hufkens, K., Milliman, T., Friedl, M. A., Frolking, S. and Richardson, A. D.: Tracking vegetation phenology across diverse biomes using Version 2.0 of the PhenoCam Dataset., Sci. Data, 6(1), 222, doi:10.1038/s41597-019-0229-9, 2019.

910 Sims, D. A., Rahman, A. F., Cordova, V. D., El-Masri, B. Z., Baldocchi, D. D., Flanagan, L. B., Goldstein, A. H., Hollinger, D. Y., Misson, L., Monson, R. K., Oechel, W. C., Schmid, H. P., Wofsy, S. C. and Xu, L.: On the use of MODIS EVI to assess gross primary productivity of North American ecosystems, J. Geophys. Res., 111(G4), doi:10.1029/2006JG000162, 2006.

Stoy, P. C., Katul, G. G., Siqueira, M. B. S., Juang, J.-Y., McCarthy, H. R., Kim, H.-S., Oishi, A. C. and Oren, R.:

915 Variability in net ecosystem exchange from hourly to inter-annual time scales at adjacent pine and hardwood forests: a wavelet analysis., Tree Physiol., 25(7), 887–902, doi:10.1093/treephys/25.7.887, 2005.

Stoy, P. C., Trowbridge, A. M. and Bauerle, W. L.: Controls on seasonal patterns of maximum ecosystem carbon uptake and canopy-scale photosynthetic light response: contributions from both temperature and photoperiod., Photosyn. Res., 119(1–2), 49–64, doi:10.1007/s11120-013-9799-0, 2014a.

920 Stoy, P., Lin, H., Novick, K., Siqueira, M. and Juang, J.-Y.: The role of vegetation on the ecosystem radiative entropy budget and trends along ecological succession, Entropy, 16(7), 3710–3731, doi:10.3390/e16073710, 2014b.

Sullivan, P., Gallagher, F. W., Boukabara, S. A., Lindsey, D. T. and Grigsby, E.: What Follows GOES-R? [online] Available from: https://ams.confex.com/ams/2020Annual/meetingapp.cgi/Paper/370685 (Accessed 24 August 2020), 2020.

Sun, D. and Pinker, R. T.: Estimation of land surface temperature from a Geostationary Operational Environmental Satellite

925 (GOES-8), J. Geophys. Res., 108(D11), 4326, doi:10.1029/2002JD002422, 2003.

Suomi, V. E. and Parent, R. J.: a color view of planet Earth, Bull. Amer. Meteor. Soc., 49(2), 74–75, doi:10.1175/1520-0477-49.2.74, 1968.

Tan, B., Dellomo, J. J., Folley, C. N., Grycewicz, T. J., Houchin, S., Isaacson, P. J., Johnson, P. D., Porter, B. C., Reth, A. D., Thiyanaratnam, P. and Wolfe, R. E.: GOES-R series image navigation and registration performance assessment tool set,

930 J. Appl. Remote Sens., 14(03), 1, doi:10.1117/1.JRS.14.032405, 2020.

Tan, B., Dellomo, J. J., Wolfe, R. E. and Reth, A. D.: GOES-16 and GOES-17 ABI INR assessment, in Earth Observing Systems XXIV, edited by J. J. Butler, X. (Jack) Xiong, and X. Gu, p. 49, SPIE., 2019.

Tan, B., Dellomo, J., Wolfe, R. E. and Reth, A. D.: GOES-16 ABI navigation assessment, in Earth Observing Systems XXIII, edited by J. J. Butler, X. (Jack) Xiong, and X. Gu, p. 15, SPIE., 2018.

935 Tian, Y., Romanov, P., Yu, Y., Xu, H. and Tarpley, D.: Analysis of vegetation index NDVI anisotropy to improve the accuracy of the GOES-R green vegetation fraction product, in 2010 IEEE International Geoscience and Remote Sensing Symposium, pp. 2091–2094, IEEE., 2010.

Tran, N. N., Huete, A., Nguyen, H., Grant, I., Miura, T., Ma, X., Lyapustin, A., Wang, Y. and Ebert, E.: Seasonal Comparisons of Himawari-8 AHI and MODIS Vegetation Indices over Latitudinal Australian Grassland Sites, Remote Sens (Basel), 12(15), 2494, doi:10.3390/rs12152494, 2020.

Trigo, I. F., Dacamara, C. C., Viterbo, P., Roujean, J.-L., Olesen, F., Barroso, C., Camacho-de-Coca, F., Carrer, D., Freitas, S. C., García-Haro, J., Geiger, B., Gellens-Meulenberghs, F., Ghilain, N., Meliá, J., Pessanha, L., Siljamo, N. and Arboleda, A.: The satellite application facility for land surface analysis, Int. J. Remote Sens., 32(10), 2725–2744, doi:10.1080/01431161003743199, 2011.

Tucker, C. J.: Red and photographic infrared linear combinations for monitoring vegetation, Remote Sensing of Environment, 8(2), 127–150, doi:10.1016/0034-4257(79)90013-0, 1979.

Tucker, C. J.: Remote sensing of leaf water content in the near infrared, Remote Sensing of Environment, 10(1), 23–32, doi:10.1016/0034-4257(80)90096-6, 1980.

Tucker, C. J., Townshend, J. R. and Goff, T. E.: African land-cover classification using satellite data., Science, 227(4685), 369–375, doi:10.1126/science.227.4685.369, 1985.

Ulivieri, C. and Cannizzaro, G.: Land surface temperature retrievals from satellite measurements, Acta Astronaut., 12(12), 977–985, doi:10.1016/0094-5765(85)90026-8, 1985.

Verger, A., Baret, F. and Weiss, M.: Near Real-Time Vegetation Monitoring at Global Scale, IEEE J. Sel. Top. Appl. Earth Observations Remote Sensing, 7(8), 3473–3481, doi:10.1109/JSTARS.2014.2328632, 2014.

Vermote, E. F., Tanre, D., Deuze, J. L., Herman, M. and Morcette, J. J.: Second Simulation of the Satellite Signal in the Solar Spectrum, 6S: an overview, IEEE Trans. Geosci. Remote Sensing, 35(3), 675–686, doi:10.1109/36.581987, 1997.

Wagner, S. C., Govaerts, Y. M. and Lattanzio, A.: Joint retrieval of surface reflectance and aerosol optical depth from MSG/SEVIRI observations with an optimal estimation approach: 2. Implementation and evaluation, J. Geophys. Res., 115(D2), doi:10.1029/2009JD011780, 2010.

Wang, M., Ahn, J.-H., Jiang, L., Shi, W., Son, S., Park, Y.-J. and Ryu, J.-H.: Ocean color products from the Korean Geostationary Ocean Color Imager (GOCI)., Opt. Express, 21(3), 3835–3849, doi:10.1364/OE.21.003835, 2013.

Wang, W., Li, S., Hashimoto, H., Takenaka, H., Higuchi, A., Kalluri, S. and Nemani, R.: An Introduction to the Geostationary-NASA Earth Exchange (GeoNEX) Products: 1. Top-of-Atmosphere Reflectance and Brightness Temperature, Remote Sens (Basel), 12(8), 1267, doi:10.3390/rs12081267, 2020.

Wang, W., Qu, J. J., Hao, X., Liu, Y. and Stanturf, J. A.: Post-hurricane forest damage assessment using satellite remote sensing, Agricultural and Forest Meteorology, 150(1), 122–132, doi:10.1016/j.agrformet.2009.09.009, 2010.

Weiss, A. and Norman, J. M.: Partitioning solar radiation into direct and diffuse, visible and near-infrared components, Agricultural and Forest Meteorology, 34(2–3), 205–213, doi:10.1016/0168-1923(85)90020-6, 1985.

Wheeler, K. I. and Dietze, M. C.: A Statistical Model for Estimating Midday NDVI from the Geostationary Operational Environmental Satellite (GOES) 16 and 17, Remote Sens (Basel), 11(21), 2507, doi:10.3390/rs11212507, 2019.

Wheeler, K. I. and Dietze, M. C.: Improving the monitoring of deciduous broadleaf phenology using the Geostationary Operational Environmental Satellite (GOES) 16 and 17, Biogeosciences Discussions, 1–24, doi:https://doi.org/10.5194/bg-2020-309, 2020.

White, M. A., de BEURS, K. M., Didan, K., Inouye, D. W., Richardson, A. D., Jensen, O. P., O'Keefe, J., Zhang, G., Nemani, R. R., van LEEUWEN, W. J. D., Brown, J. F., de WIT, A., Schaepman, M., Lin, X., Dettinger, M., Bailey, A. S., Kimball, J., Schwartz, M. D., Baldocchi, D. D., Lee, J. T. and Lauenroth, W. K.: Intercomparison, interpretation, and assessment of spring phenology in North America estimated from remote sensing for 1982-2006., Glob. Chang. Biol., 15(10), 2335–2359, doi:10.1111/j.1365-2486.2009.01910.x, 2009.

Whittaker, T.: GOES-16 ABI Parallax: CONUS Sector, [online] Available from: http://cimss.ssec.wisc.edu/goes/webapps/parallax/goes16_conus.html (Accessed 25 June 2020), 2014.

Wiesner, S., Staudhammer, C. L., Stoy, P. C., Boring, L. R. and Starr, G.: Quantifying energy use efficiency via entropy production: a case study from longleaf pine ecosystems, Biogeosciences, 16(8), 1845–1863, doi:10.5194/bg-16-1845-2019, 2019.

Williams, M., Richardson, A. D., Reichstein, M., Stoy, P. C., Peylin, P., Verbeeck, H., Carvalhais, N., Jung, M., Hollinger, D. Y., Kattge, J., Leuning, R., Luo, Y., Tomelleri, E., Trudinger, C. M. and Wang, Y. P.: Improving land surface models with FLUXNET data, Biogeosciences, 6(7), 1341–1359, doi:10.5194/bg-6-1341-2009, 2009.

Wong, C. Y. S., D'Odorico, P., Bhathena, Y., Arain, M. A. and Ensminger, I.: Carotenoid based vegetation indices for accurate monitoring of the phenology of photosynthesis at the leaf-scale in deciduous and evergreen trees, Remote Sensing of Environment, 233, 111407, doi:10.1016/j.rse.2019.111407, 2019.

Wooster, M.: Fire radiative energy for quantitative study of biomass burning: derivation from the BIRD experimental satellite and comparison to MODIS fire products, Remote Sensing of Environment, 86(1), 83–107, doi:10.1016/S0034-4257(03)00070-1, 2003.

Wu, G., Guan, K., Jiang, C., Peng, B., Kimm, H., Chen, M., Yang, X., Wang, S., Suyker, A. E., Bernacchi, C. J., Moore, C. E., Zeng, Y., Berry, J. A. and Cendrero-Mateo, M. P.: Radiance-based NIRv as a proxy for GPP of corn and soybean, Environmental Research Letters, 15(3), 034009, doi:10.1088/1748-9326/ab65cc, 2020.

Wu, P., Shen, H., Zhang, L. and Göttsche, F.-M.: Integrated fusion of multi-scale polar-orbiting and geostationary satellite observations for the mapping of high spatial and temporal resolution land surface temperature, Remote Sensing of Environment, 156, 169–181, doi:10.1016/j.rse.2014.09.013, 2015.

Xiao, J., Chevallier, F., Gomez, C., Guanter, L., Hicke, J. A., Huete, A. R., Ichii, K., Ni, W., Pang, Y., Rahman, A. F., Sun, G., Yuan, W., Zhang, L. and Zhang, X.: Remote sensing of the terrestrial carbon cycle: A review of advances over 50 years., Remote Sens. Environ., 233, 111383, doi:10.1016/j.rse.2019.111383, 2019.

Xu, W., Wooster, M. J., Roberts, G. and Freeborn, P.: New GOES imager algorithms for cloud and active fire detection and fire radiative power assessment across North, South and Central America, Remote Sensing of Environment, 114(9), 1876–1895, doi:10.1016/j.rse.2010.03.012, 2010.

Xu, X., Riley, W. J., Koven, C. D., Jia, G. and Zhang, X.: Earlier leaf-out warms air in the north, Nat. Clim. Chang., doi:10.1038/s41558-020-0713-4, 2020.

Yang, Y., Anderson, M. C., Gao, F., Wardlow, B., Hain, C. R., Otkin, J. A., Alfieri, J., Yang, Y., Sun, L. and Dulaney, W.: Field-scale mapping of evaporative stress indicators of crop yield: An application over Mead, NE, USA, Remote Sensing of Environment, 210, 387–402, doi:10.1016/j.rse.2018.02.020, 2018.

Yan, D., Zhang, X., Yu, Y. and Guo, W.: A Comparison of Tropical Rainforest Phenology Retrieved From Geostationary (SEVIRI) and Polar-Orbiting (MODIS) Sensors Across the Congo Basin, IEEE Trans. Geosci. Remote Sensing, 54(8), 4867–4881, doi:10.1109/TGRS.2016.2552462, 2016.

Yeom, J.-M., Jeong, S., Jeong, G., Ng, C. T., Deo, R. C. and Ko, J.: Monitoring paddy productivity in North Korea employing geostationary satellite images integrated with GRAMI-rice model., Sci. Rep., 8(1), 16121, doi:10.1038/s41598-018-34550-0, 2018.

Yeom, J.-M. and Kim, H.-O.: Comparison of NDVIs from GOCI and MODIS Data towards Improved Assessment of Crop Temporal Dynamics in the Case of Paddy Rice, Remote Sens (Basel), 7(9), 11326–11343, doi:10.3390/rs70911326, 2015.

Yeom, J.-M., Ko, J. and Kim, H.-O.: Application of GOCI-derived vegetation index profiles to estimation of paddy rice yield using the GRAMI rice model, Computers and Electronics in Agriculture, 118, 1–8, doi:10.1016/j.compag.2015.08.017, 2015.

Yeom, J.-M., Roujean, J.-L., Han, K.-S., Lee, K.-S. and Kim, H.-W.: Thin cloud detection over land using background surface reflectance based on the BRDF model applied to Geostationary Ocean Color Imager (GOCI) satellite data sets, Remote Sensing of Environment, 239, 111610, doi:10.1016/j.rse.2019.111610, 2020.

Yuan, W., Liu, S., Zhou, G., Zhou, G., Tieszen, L. L., Baldocchi, D., Bernhofer, C., Gholz, H., Goldstein, A. H., Goulden, M. L., Hollinger, D. Y., Hu, Y., Law, B. E., Stoy, P. C., Vesala, T. and Wofsy, S. C.: Deriving a light use efficiency model from eddy covariance flux data for predicting daily gross primary production across biomes, Agricultural and Forest Meteorology, 143(3–4), 189–207, doi:10.1016/j.agrformet.2006.12.001, 2007.

Yu, F., Wu, X., Yoo, H., Wang, Z., Qian, H. and Shao, X.: Radiometric calibration performance of GOES-17 Advanced Baseline Imager (ABI), in Earth Observing Systems XXIV, edited by J. J. Butler, X. (Jack) Xiong, and X. Gu, p. 48, SPIE., 2019.

Yu, Y., Tarpley, D., Privette, J. L., Goldberg, M. D., Rama Varma Raja, M. K., Vinnikov, K. Y. and Hui Xu: Developing Algorithm for Operational GOES-R Land Surface Temperature Product, IEEE Trans. Geosci. Remote Sensing, 47(3), 936–951, doi:10.1109/TGRS.2008.2006180, 2009.

Yu, Y., Tarpley, D. and Xu, H.: GOES-R Advanced Baseline Imager (ABI) Algorithm Theoretical Basis Document For Land Surface Temperature (Version 2.5), NOAA NESDIS CENTER for SATELLITE APPLICATIONS and RESEARCH., 2012.

Zakšek, K., Hort, M., Zaletelj, J. and Langmann, B.: Monitoring volcanic ash cloud top height through simultaneous retrieval of optical data from polar orbiting and geostationary satellites, Atmospheric Chemistry and Physics, 13(5), 2589–2606, doi:10.5194/acp-13-2589-2013, 2013.

Zeng, L., Wardlow, B. D., Xiang, D., Hu, S. and Li, D.: A review of vegetation phenological metrics extraction using time-series, multispectral satellite data, Remote Sensing of Environment, 237, 111511, doi:10.1016/j.rse.2019.111511, 2020.

Zhang, X., Friedl, M. A., Schaaf, C. B., Strahler, A. H., Hodges, J. C. F., Gao, F., Reed, B. C. and Huete, A.: Monitoring vegetation phenology using MODIS, Remote Sensing of Environment, 84(3), 471–475, doi:10.1016/S0034-4257(02)00135-9, 2003.

Zhang, X., Kondragunta, S., Ram, J., Schmidt, C. and Huang, H.-C.: Near-real-time global biomass burning emissions product from geostationary satellite constellation, J. Geophys. Res., 117(D14), doi:10.1029/2012JD017459, 2012.

Zhang, X., Liang, S., Zhou, G., Wu, H. and Zhao, X.: Generating Global LAnd Surface Satellite incident shortwave radiation and photosynthetically active radiation products from multiple satellite data, Remote Sensing of Environment, 152, 318–332, doi:10.1016/j.rse.2014.07.003, 2014.

Zhao, J., Chen, X., Zhang, J., Zhao, H. and Song, Y.: Higher temporal evapotranspiration estimation with improved SEBS model from geostationary meteorological satellite data., Sci. Rep., 9(1), 14981, doi:10.1038/s41598-019-50724-w, 2019.

Zhao, M., Heinsch, F. A., Nemani, R. R. and Running, S. W.: Improvements of the MODIS terrestrial gross and net primary production global data set, Remote Sensing of Environment, 95(2), 164–176, doi:10.1016/j.rse.2004.12.011, 2005.

Zhao, W. and Duan, S.-B.: Reconstruction of daytime land surface temperatures under cloud-covered conditions using integrated MODIS/Terra land products and MSG geostationary satellite data, Remote Sensing of Environment, 247, 111931, doi:10.1016/j.rse.2020.111931, 2020.

Zheng, T., Liang, S. and Wang, K.: Estimation of Incident Photosynthetically Active Radiation from GOES Visible Imagery, J. Appl. Meteor. Climatol., 47(3), 853–868, doi:10.1175/2007JAMC1475.1, 2008.

Zhou, Y., Zhang, L., Xiao, J., Chen, S., Kato, T. and Zhou, G.: A Comparison of Satellite-Derived Vegetation Indices for Approximating Gross Primary Productivity of Grasslands, Rangeland Ecology & Management, 67(1), 9–18, doi:10.2111/REM-D-13-00059.1, 2014.

Zscheischler, J., Fatichi, S., Wolf, S., Blanken, P. D., Bohrer, G., Clark, K., Desai, A. R., Hollinger, D., Keenan, T., Novick, K. A. and Seneviratne, S. I.: Short-term favorable weather conditions are an important control of interannual variability in carbon and water fluxes., J. Geophys. Res. Biogeosci., 121(8), 2186–2198, doi:10.1002/2016JG003503, 2016.

https://doi.org/10.5194/bg-2020-454
Preprint. Discussion started: 8 January 2021

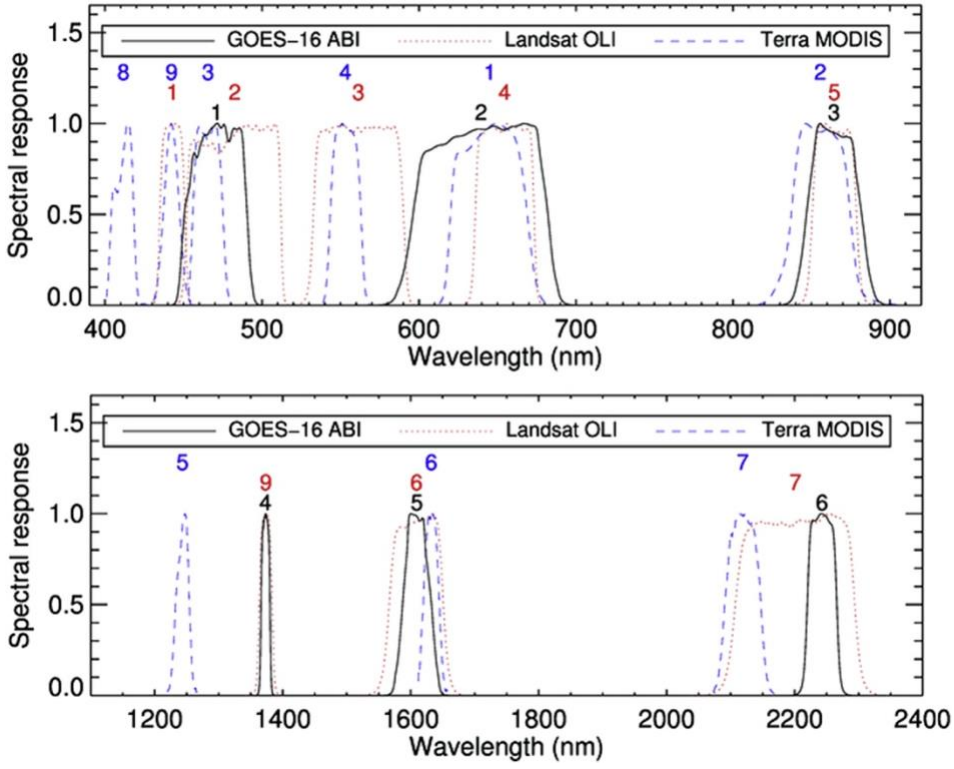

Figure 1: A comparison of the spectral sensitivity of the Advanced Baseline Imager (ABI) with the Landsat Operational Land Imager (OLI) and MODIS Terra (McCorkel et al., 2020).

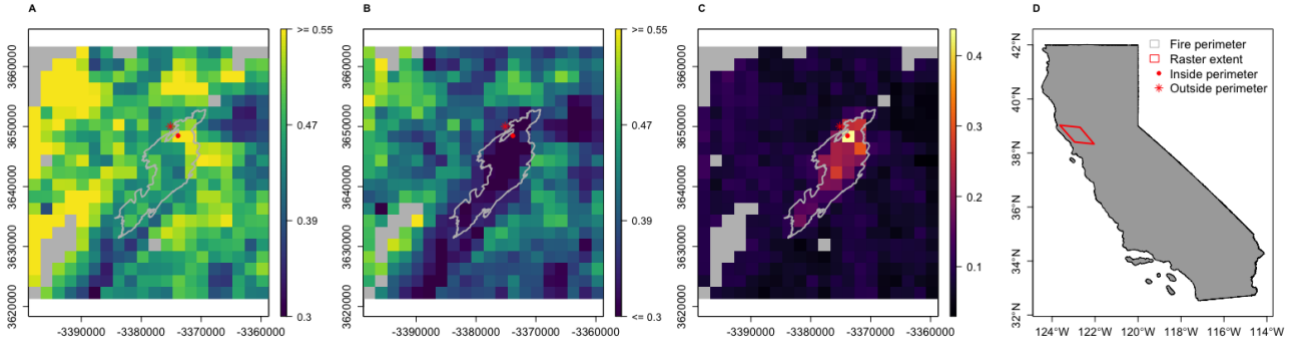

Figure 2: Top-of-Atmosphere (TOA) Normalized Difference Vegetation Index (NDVI) calculated using TOA reflectance factor from GOES-16 imagery for (a) Oct. 22, 2019, 21:00 UTC and (b) Nov. 8, 2019, 21:00 UTC and their difference (c) for the Kincade fire perimeter in northern California (d) (Oct. 23, 2019). Gray pixels were identified as cloudy from the GOES Clear Sky Mask. The points inside and outside of the fire perimeter correspond to the time series in Fig. 3 and Fig. 4.

https://doi.org/10.5194/bg-2020-454
Preprint. Discussion started: 8 January 2021

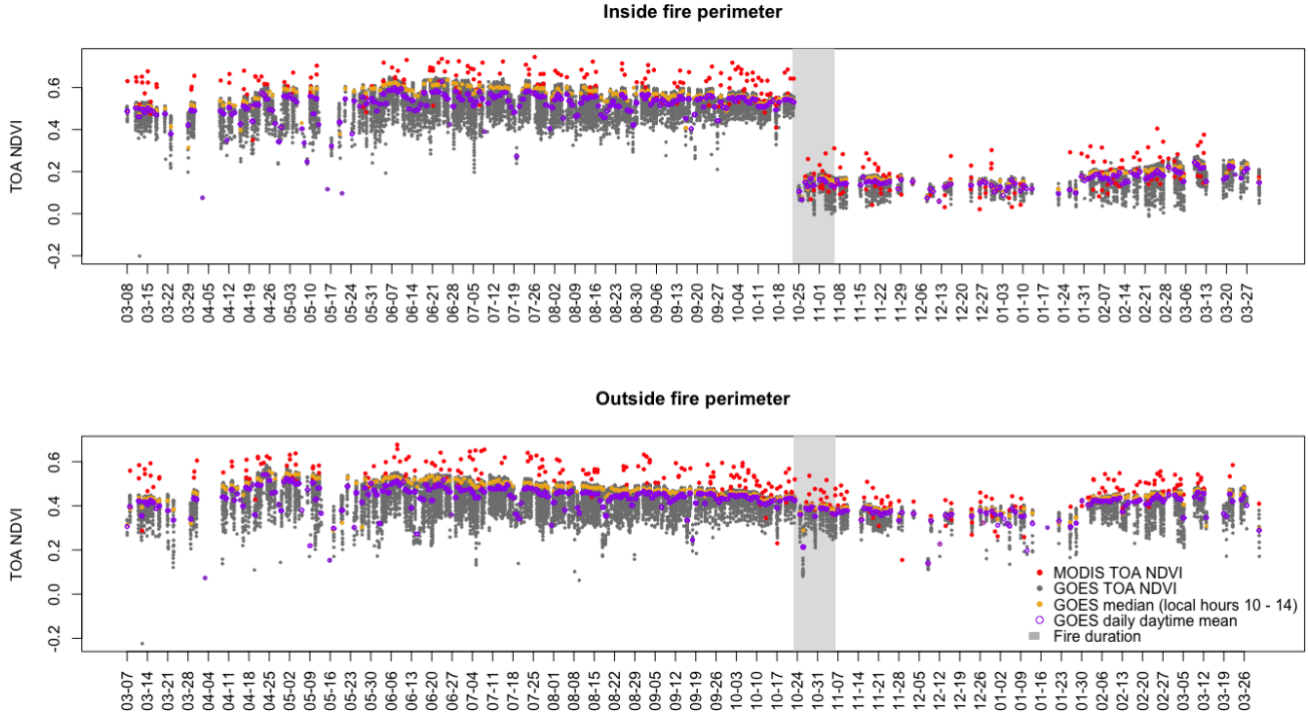

Figure 3: Top-of-Atmosphere (TOA) Normalized Difference Vegetation Index (NDVI) calculated using TOA reflectance factor from ABI on GOES-16 and MODIS on the Terra and Aqua satellites for pixels inside and outside the Kincade fire (Oct. 23, 2019) perimeter in northern California for the period March 2019 to March 2020. The GOES Clear Sky Mask was applied to observations from GOES and MODIS. All observations are daytime with solar zenith angle < 70°. The locations of the points inside and outside of the fire perimeter are displayed in Fig. 2.

https://doi.org/10.5194/bg-2020-454
Preprint. Discussion started: 8 January 2021

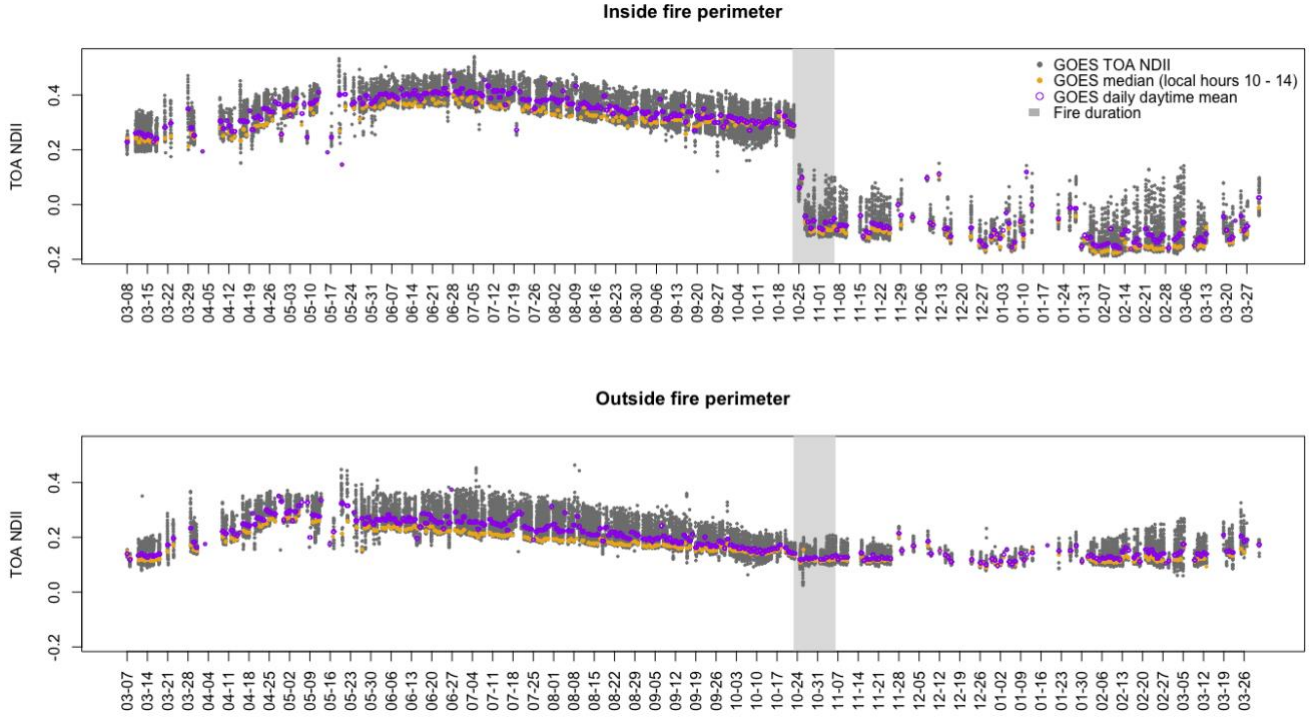

Figure 4: Top-of-Atmosphere (TOA) Normalized Difference Infrared Index (NDII) calculated using TOA reflectance factor from ABI on GOES-16 for pixels inside and outside the Kincade fire (Oct. 23, 2019) perimeter in northern California for the period March 2019 to March 2020. The GOES Clear Sky Mask was applied to observations from GOES. All observations are daytime with solar zenith angle < 70°. The locations of the points inside and outside of the fire perimeter are displayed in Fig. 2.

https://doi.org/10.5194/bg-2020-454
Preprint. Discussion started: 8 January 2021

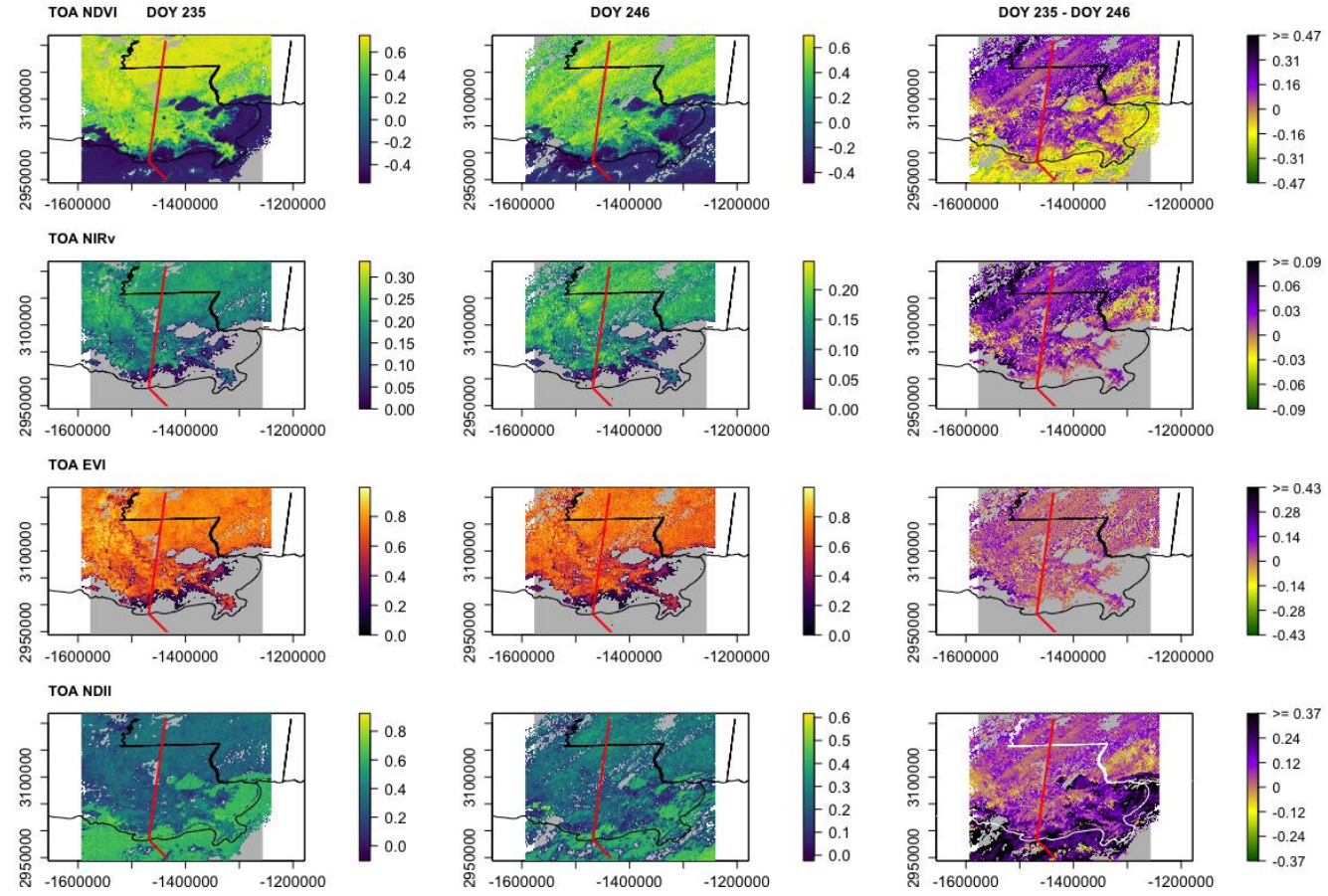

Figure 5: Top-of-Atmosphere (TOA) Normalized Difference Vegetation Index (NDVI), near-infrared reflectance of vegetation (NIRv), Enhanced Vegetation Index (EVI) and Normalized Difference Infrared Index (NDII) calculated using TOA reflectance factors from GOES-16 imagery for day of year (DOY) 235 (Aug. 22, 2020) 16:00 UTC, DOY 246 (Sep. 2, 2019) 16:00 UTC and their difference around the advisory track for Hurricane Laura (red line) in southern Louisiana (Aug. 26, 2020, DOY 239). Gray pixels represent cloudy pixels from the GOES Clear Sky Mask or vegetation index values below 0 for NIRv and EVI.

https://doi.org/10.5194/bg-2020-454
Preprint. Discussion started: 8 January 2021

Table 1: Instrument characteristics for the GOES-R Advanced Baseline Imager, Advanced Himawari Imager on Himawari-8/9, and the Advanced Meteorological Imager on the Geostationary - Korea Multi-Purpose Satellite-2 (GEO-KOMPAST-2A) (a) and The Global Ocean Color Imager-II (GOCI-II) on GEO-KOMPSAT-2B (b)

a.

GOES-16/17 Advanced Baseline Imager (ABI)			**Himawari-8/9 Advanced Himawari Imager (AHI)**			**GEO-KOMPSAT 2A Advanced Meteorological Imager (AMI)**		
Band	**Central Wavelength (µm)**	**Spatial Resolution (km)**	**Band**	**Central Wavelength (µm)**	**Spatial Resolution (km)**	**Band**	**Central Wavelength (µm)**	**Spatial Resolution (km)**
1	0.47	1	1	0.47	1	1	0.47	1
			2	0.51	1	2	0.51	1
2	0.64	0.5	3	0.64	0.5	3	0.64	0.5
3	0.86	1	4	0.86	1	4	0.86	1
4	1.37	2				5	1.4	2
5	1.6	1	5	1.6	2	6	1.6	2
6	2.2	2	6	2.3	2			
7	3.9	2	7	3.9	2	7	3.8	2
8	6.2	2	8	6.2	2	8	6.2	2
9	6.9	2	9	6.9	2	9	6.9	2
10	7.3	2	10	7.3	2	10	7.3	2
11	8.4	2	11	8.6	2	11	8.6	2
12	9.6	2	12	9.6	2	12	9.6	2
13	10.3	2	13	10.4	2	13	10.4	2
14	11.2	2	14	11.2	2	14	11.2	2
15	12.3	2	15	12.4	2	15	12.4	2
16	13.3	2	16	13.3	2	16	13.3	2

https://doi.org/10.5194/bg-2020-454
Preprint. Discussion started: 8 January 2021

b.

GEO-KOMPSAT-2B Global Ocean Color Imager-II (CGOCI-II)		
Band	**Central Wavelength (nm)**	**Spatial Resolution (m)**
1	380	250
2	412	250
3	443	250
4	490	250
5	510	250
6	555	250
7	620	250
8	660	250
9	680	250
10	709	250
11	745	250
12	865	250
13	Wideband	250